Research Square

Preprints are preliminary reports that have not undergone peer review.
They should not be considered conclusive, used to inform clinical practice,
or referenced by the media as validated information.

Development of a Prognostic Index for Clear Cell Renal Cell Carcinoma Using Machine Learning and Multi-omics Analysis to Enhance Clinical Outcomes and Drug Sensitivity

Feifan Tang
the Nanxishan Hospital of Guangxi Zhuang Autonomous Region
songbai Liao
1182194916@qq.com

the Nanxishan Hospital of Guangxi Zhuang Autonomous Region
xianliang Hou
the Second Affiliated Hospital of Guilin Medical University
biao Zhang
the Second Affiliated Hospital of Guilin Medical University

Research Article

Keywords: Clear-cell renal carcinoma, Driver gene signature, Machine-learning model, Prognostic index, Immunotherapy, Drug response

Posted Date: August 3rd, 2026

DOI: https://doi.org/10.21203/rs.3.rs-10277358/v1

License: This work is licensed under a Creative Commons Attribution 4.0 International License.
Read Full License

Additional Declarations: No competing interests reported.

Development of a Prognostic Index for Clear Cell Renal Cell Carcinoma Using Machine Learning and Multi-omics Analysis to Enhance Clinical Outcomes and Drug Sensitivity

Feifan Tang[1], Songbai Liao[1]*, Xianliang Hou[2]*, Biao Zhang[2]

*Corresponding author:

Songbai Liao, Department of Urology, the Nanxishan Hospital of Guangxi Zhuang Autonomous Region, Guilin 541002, China. E-mail: 1182194916@qq.com

Xianliang Hou, Research Administration Office, the Second Affiliated Hospital of Guilin Medical University, Guilin, 541199, China. E-mail: houxl115@126.com

Abstract

Background: Clear cell renal cell carcinoma (KIRC) represents the major malignant subtype of kidney cancer and shows pronounced biological heterogeneity. For patients with advanced disease, therapeutic resistance and the lack of stable prognostic markers continue to keep 5-year survival below 15%. Cancer driver genes (CDGs) participate in malignant transformation and tumor progression, but their combined prognostic value in KIRC has not been fully clarified.

Methods: We assembled a catalogue of 6,291 CDGs and designed a machine-learning-based workflow to build a Cancer Driver Gene Prognostic Index (CDPI). The analysis integrated differential expression screening, consensus clustering, WGCNA, and four feature-selection algorithms, including Lasso, decision tree, random forest, and XGBoost. Model performance was examined in the TCGA-KIRC training set and then tested in the external E-MTAB-1980 cohort.

Results: Differential expression screening yielded 5,243 DECDRGs and four recurrent core DECDRGs. Based on consensus clustering, KIRC samples were separated into two molecular groups, and the C1 group showed poorer survival. WGCNA selected the turquoise module as the cluster-associated module, from which 148 key DECDRGs were obtained; 105 of these genes were significant in univariate Cox analysis. Cross-model feature selection ultimately produced a CDPI composed of five genes: PLCL1, GABRB3, USP46, RNF152, and PFKP. Patients with higher CDPI values had shorter overall survival in both datasets. The CDPI-based nomogram achieved good prediction accuracy, including a 1-year AUC of 0.86, and showed a favorable decision-curve profile. High CDPI was also accompanied by stronger immune infiltration, lower tumor purity, and different mutation patterns. Drug-response prediction suggested increased sensitivity to gemcitabine, epirubicin, ULK1 inhibitors, docetaxel, and AZD7762, but reduced sensitivity to Daporinad, osimertinib, and cediranib.

Conclusion: The CDPI may serve as a practical stratification index for KIRC and may help interpret immune escape and treatment vulnerability, although prospective clinical confirmation is still required.

Keywords

Clear-cell renal carcinoma; Driver gene signature; Machine-learning model; Prognostic index; Immunotherapy; Drug response

Introduction

Clear cell renal cell carcinoma (KIRC) accounts for approximately 70%-80% of renal cell carcinoma cases and is the most common pathological subtype. Its clinical behavior is shaped by marked molecular diversity and aggressive progression, both of which contribute to high mortality[2]. Although imaging and surgical techniques have improved, patients with advanced-stage KIRC still have poor outcomes, with 5-year survival remaining below 15%[3]. Current treatment options include surgery, tyrosine kinase inhibitor-based targeted therapy, and immune checkpoint blockade directed at the PD-1/PD-L1 axis. However, many patients show primary or acquired resistance, and tumor immune evasion further limits therapeutic benefit. Reliable markers that can classify prognostic risk and anticipate treatment response are therefore needed for individualized KIRC management.

Cancer development is driven by accumulated genomic alterations in genes that confer growth and survival advantages. In KIRC, loss or mutation of von Hippel-Lindau (VHL) is central to pathogenesis and strongly influences metabolic rewiring and the immune milieu. Other driver events, including alterations in PBRM1, may also shape responsiveness to immunotherapy. Although several individual CDGs have been investigated, the broader CDG expression program in KIRC remains incompletely characterized. Many published signatures do not explicitly incorporate driver-gene biology or its interaction with the tumor immune microenvironment. A systematic CDG-centered expression analysis may therefore provide a route to prognostic models that better reflect the oncogenic biology of clear cell renal cell carcinoma.

To address this issue, we integrated multi-omics data with computational modeling. Transcriptomic and clinical information from TCGA and ArrayExpress were analyzed through a stepwise pipeline involving differential expression screening, PPI network analysis, molecular clustering, WGCNA, and machine-learning feature selection. Lasso, decision tree, random forest, and XGBoost were jointly used to refine candidate genes. This workflow led to a five-gene cancer driver gene prognostic index (CDPI) based on PLCL1, PFKP, GABRB3, USP46, and RNF152.

This study had three aims. The first was to establish a measurable CDPI capable of separating KIRC patients into prognostically distinct risk groups. The second was to examine how the CDPI relates to immune infiltration, checkpoint expression, and immune escape. The third was to determine whether CDPI could help predict sensitivity to commonly used chemotherapeutic or targeted agents. Together, these analyses were intended to provide a CDG-based molecular tool for prognosis and treatment selection in KIRC.

Materials And Methods

Data Collection

The workflow is summarized in Figure S1. RNA-seq count data, survival information, and clinical annotations for 529 KIRC tumors and 59 normal kidney samples were downloaded from TCGA (https://portal.gdc.cancer.gov/) and used as the training cohort[6]. E-MTAB-1980 (N = 101), obtained from ArrayExpress (https://www.ebi.ac.uk/biostudies/ArrayExpress), served as the validation cohort[10]. A total of 6,291 CDGs were collected from GeneCards (https://www.genecards.org/) for downstream analyses[11].

Differential Expression and PPI Network Analysis

The R package "limma"[12] was used for differential expression analysis. Genes meeting $|\log2FC| > 1$ and adjusted $P < 0.05$ were retained as DECDRGs. Protein interactions for these genes were queried in STRING[13] and the resulting PPI network was displayed in Cytoscape (v3.9.0)[14]. MCODE was then applied to extract network modules using degree cutoff = 2, node score cutoff = 0.2, k-core = 2, and maximum depth = 100. Hub candidates were ranked with the EPC, BottleNeck, Degree, and MNC algorithms in Cytohubba[16]. NetworkAnalyst 3.0 and the JASPAR database were used to infer transcription factors for the core genes. GO[19] and KEGG[20] analyses were subsequently used for functional interpretation.

Examination of the Tumor Immune Microenvironment

Immune infiltration was quantified with the "IOBR" R package[21] by applying MCP-counter[22], EPIC[23], xCell[24], CIBERSORT[25], IPS[26], quanTIseq[27], ESTIMATE[28], TIMER[29], and ssGSEA[30]. The ssGSEA implementation used 29 immune-related gene sets covering immune cell subsets, immune functions, pathways, and checkpoints. TIDE was used to infer immune escape and potential benefit from immune checkpoint inhibitors[31]. IPS values from TCIA were used for additional assessment of anti-PD-1 and anti-CTLA-4 response potential[26].

Consensus Clustering

The core DECDRG expression matrix was analyzed with "ConsensusClusterPlus"[32]. Candidate cluster numbers from $k = 2$ to $k = 6$ were tested, and molecular subtypes were assigned in the TCGA-KIRC cohort according to the expression of the four shared hub DECDRGs. Survival differences among clusters were evaluated with the "survival" R package.

WGCNA is a systems-biology approach that organizes genes into co-expression modules and summarizes each module by an eigengene or hub-gene structure. Linking these modules to sample traits can reveal coordinated expression programs that may contain biomarkers or therapeutic targets.

The "WGCNA" R package[33,34] was used to search for DECDRG modules related to the

clusters. After selecting a suitable soft-thresholding power, we built a scale-free co-expression network[33]. The adjacency matrix was transformed into a topological overlap matrix, from which the TOM-based dissimilarity matrix was calculated[33]. Modules were defined with dynamic tree cutting[33]. Among the 13 modules, the turquoise module was selected for further study because it showed the strongest negative association with the clusters[33]. Genes with high GS and MM values were regarded as key DECDRGs[34].

Construction and Validation of the CDPI

From the 105 DECDRGs associated with survival in univariate Cox analysis, candidate prognostic genes were filtered with four algorithms: Lasso Cox regression (glmnet; elastic net alpha = 0.2-0.3; lambda.min chosen by ten-fold cross-validation), XGBoost (xgboost; objective = 'survival cox'; 6:4 split; max_depth = 5, eta = 0.01, subsample = 0.8, colsample_bytree = 0.8; early stopping after 30 rounds; Gain metric), random forest (randomForestSRC; log-rank splitting; ntree = 1000-2000, mtry = sqrt(p), nodesize = 15; frequency ranking over 50 repetitions), and decision tree (rpart; method = 'exp', minsplit = 20, cp = 0.01, ten-fold cross-validation; variable importance). Feature scores were scaled by Min-Max normalization and combined with equal weights. The 15 highest-ranked genes were entered into exhaustive multivariate Cox combination screening[39], which selected PLCL1, GABRB3, USP46, RNF152, and PFKP as independent predictors. The CDPI formula was then defined from the multivariate Cox coefficients:

$$\mathrm{CDPI} = (-0.3771) \times \mathrm{expr}(\mathrm{PLCL1}) + (-0.2361) \times \mathrm{expr}(\mathrm{PFKP}) + (-0.1743) \times \mathrm{expr}(\mathrm{GABRB3}) + (0.3489) \times \mathrm{expr}(\mathrm{USP46}) + (-0.2030) \times \mathrm{expr}(\mathrm{RNF152})$$

where expr() denotes the gene expression value ($\log_2(\mathrm{TPM} + 1)$).

The cohort was split into high- and low-CDPI groups at the median CDPI. Kaplan-Meier curves generated with the "survival" R package were used to compare survival in the TCGA-KIRC and E-MTAB-1980 cohorts. The independent prognostic value of CDPI was examined by both univariate and multivariate Cox regression.

Construction of the nomogram

Age, sex, clinical stage, and CDPI were entered into multivariate Cox regression with stepwise selection to construct a prognostic nomogram. The "rms" package was used to draw the nomogram and calibration curves. Time-dependent ROC curves were calculated with "timeROC"[40]. CDPI-related correlation and stratified analyses were then performed according to available clinical variables, and DCA was used to compare the nomogram with a clinical-variable-only model[41].

GSEA tests whether members of a predefined gene set tend to appear at the extremes of a ranked expression list more often than expected by chance.

"clusterProfiler"[42] and "enrichplot" were used for GSEA. Enriched terms were screened with $|\mathrm{NES}| > 1$ and adjusted $P < 0.05$. Hallmark (H) and ontology (C5) gene sets were used as the reference collections.

Drug Sensitivity Analysis

Drug response was inferred with "oncoPredict"[43], which maps patient expression profiles onto cancer cell-line pharmacogenomic data to estimate IC50 values. Wilcoxon tests were used to compare predicted drug sensitivity between CDPI groups. Associations between the five signature genes and drug sensitivity were further explored through GDSC and CTRP data in GSCALite[44].

Mutational Landscape Analysis

TCGA somatic mutation data for KIRC were downloaded through "TCGAbiolinks"[45]. Mutation landscapes for the two CDPI groups were visualized as waterfall plots with "Maftools"[46]. Co-occurrence and mutual-exclusivity patterns were compared for frequently mutated genes.

Assessment of Immunotherapy Efficacy

TCIA (https://tcia.at/home)[26] was used to approximate the likelihood of response to immune checkpoint blockade. The relationship between CDPI and IPS was then examined under anti-PD-1 and anti-CTLA-4 therapy settings.

Immunohistochemical Analysis

Immunohistochemistry images from the Human Protein Atlas were reviewed to compare the protein-level expression of characteristic DECDRGs between KIRC and normal tissue.

Statistical Analysis

Kaplan-Meier plots were produced with "survminer", and log-rank tests were used to compare OS between CDPI groups. Wilcoxon tests were applied to two-group comparisons, and Kruskal-Wallis tests were used for comparisons involving more than two groups. Spearman analysis was performed for correlation testing. $P <= 0.05$ was considered statistically significant. All statistical analyses were performed with R v4.5.0.

Result

Identification of Differentially Expressed Cancer Driver-Related Genes

Relative to normal kidney tissue, KIRC samples contained 5,243 DECDRGs, including 2,713 upregulated and 2,530 downregulated genes (Figure 1A). Intersecting these genes with the CDG list identified 1,359 overlapping candidates (Figure 1B). The STRING-derived PPI network was visualized in Cytoscape (v3.9.0) and showed dense interactions among the DECDRGs (Figure S2). Four Cytohubba ranking methods (Degree, EPC, BottleNeck, and MNC) converged on five core DECDRGs (Figure 1C). Regulatory transcription factors for EGFR, CD44, MYC, and GAPDH were predicted through NetworkAnalyst 3.0 using JASPAR (Figure 1D). These four core genes showed higher mRNA expression in KIRC than in normal tissue (Figure S4B). GO terms were

enriched for peptidyl-tyrosine phosphorylation, inflammatory-response regulation, leukocyte proliferation, and protein tyrosine kinase activity (Figure 1E-F). KEGG analysis highlighted pathways in cancer, cytokine-cytokine receptor interaction, central carbon metabolism in cancer, HIF-1 signaling, and PI3K-Akt signaling (Figure 1G). HPA staining patterns are shown in Figure S4A, and protein expression differences between normal and KIRC tissues were visually apparent.

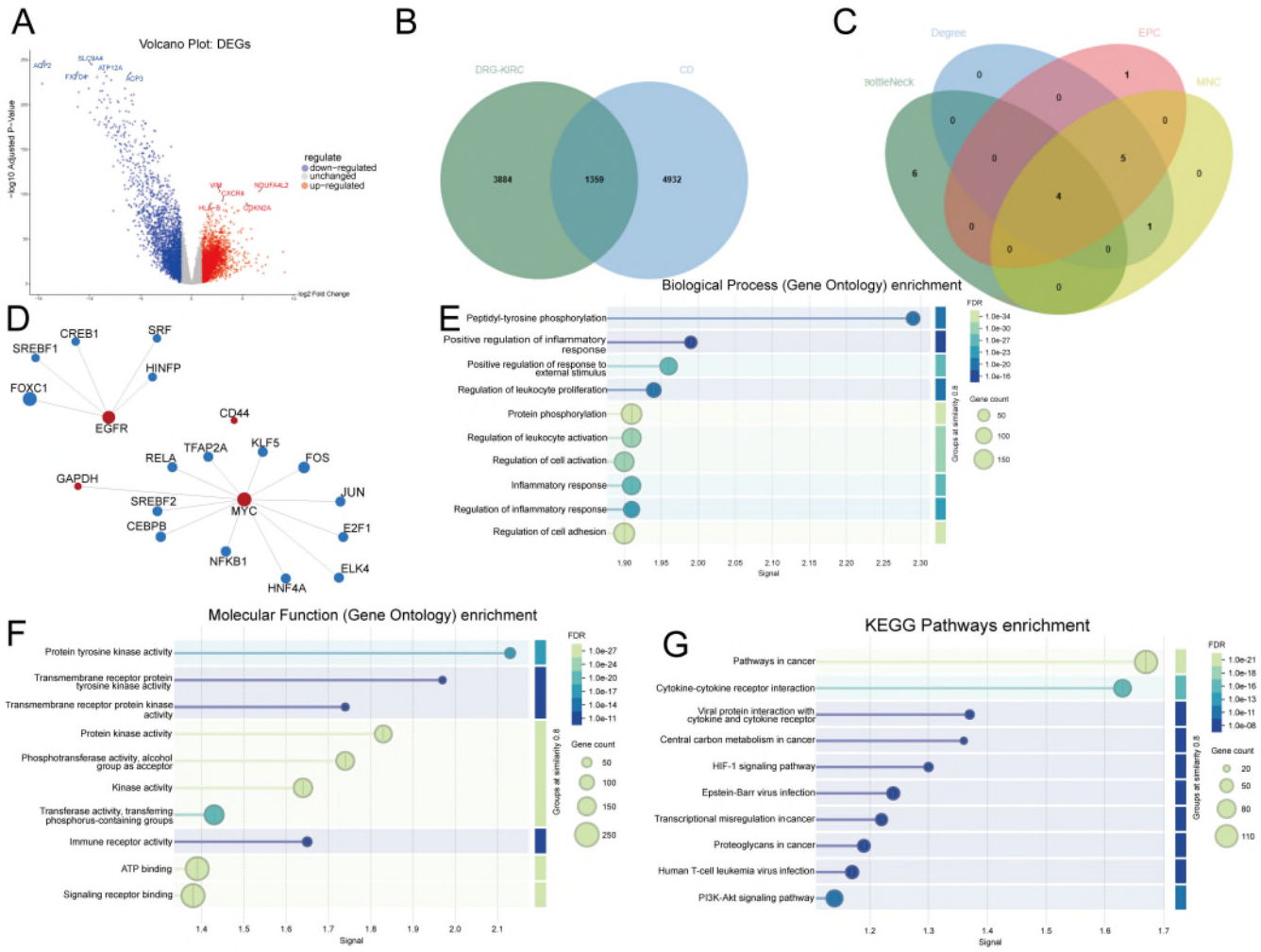


Figure 1. Differentially expressed cancer driver-related genes (DECDRGs). (**A**) Volcano plot comparing KIRC tumor samples with normal tissues; red and blue points indicate upregulated and downregulated genes, respectively. (B) Venn plot showing overlap between KIRC differentially expressed genes (DRG-KIRC) and the CD database. (**C**) Shared core DECDRGs selected by Degree, EPC, BottleNeck, and MNC in Cytohubba. (**D**) JASPAR-based transcription factor network generated in NetworkAnalyst 3.0. Red nodes denote core genes and blue nodes denote transcription factors. (**E**) GO biological process results. (**F**) GO molecular function results. (**G**) KEGG pathway enrichment results. Bubble size denotes gene count, and color indicates FDR.

Identification of Cancer Driver Gene-Related Subgroups

Using the expression profiles of four core differentially expressed genes, consensus clustering was applied to 529 KIRC samples across k = 2-6. The CDF curves supported k = 2 as the most stable solution, with high within-cluster consistency and limited overlap between clusters (Figure

2A-C). Clinical features of C1 and C2 are summarized in Table 1. The C1 subgroup had significantly shorter OS than C2 (P = 0.00011; Figure 2D). Immune-related scoring showed higher T cell dysfunction and TIDE scores in C2, whereas C1 had higher MSI scores and tumor purity. T cell exclusion, ESTIMATE, and stromal scores did not differ significantly between clusters. ssGSEA revealed broader immune-cell infiltration in C1 than in C2 (Figure 2M-N). To test the robustness of these immune findings, six additional algorithms, MCP-counter, EPIC, xCell, CIBERSORT, quanTIseq, and TIMER, were used for validation (Figure S5).

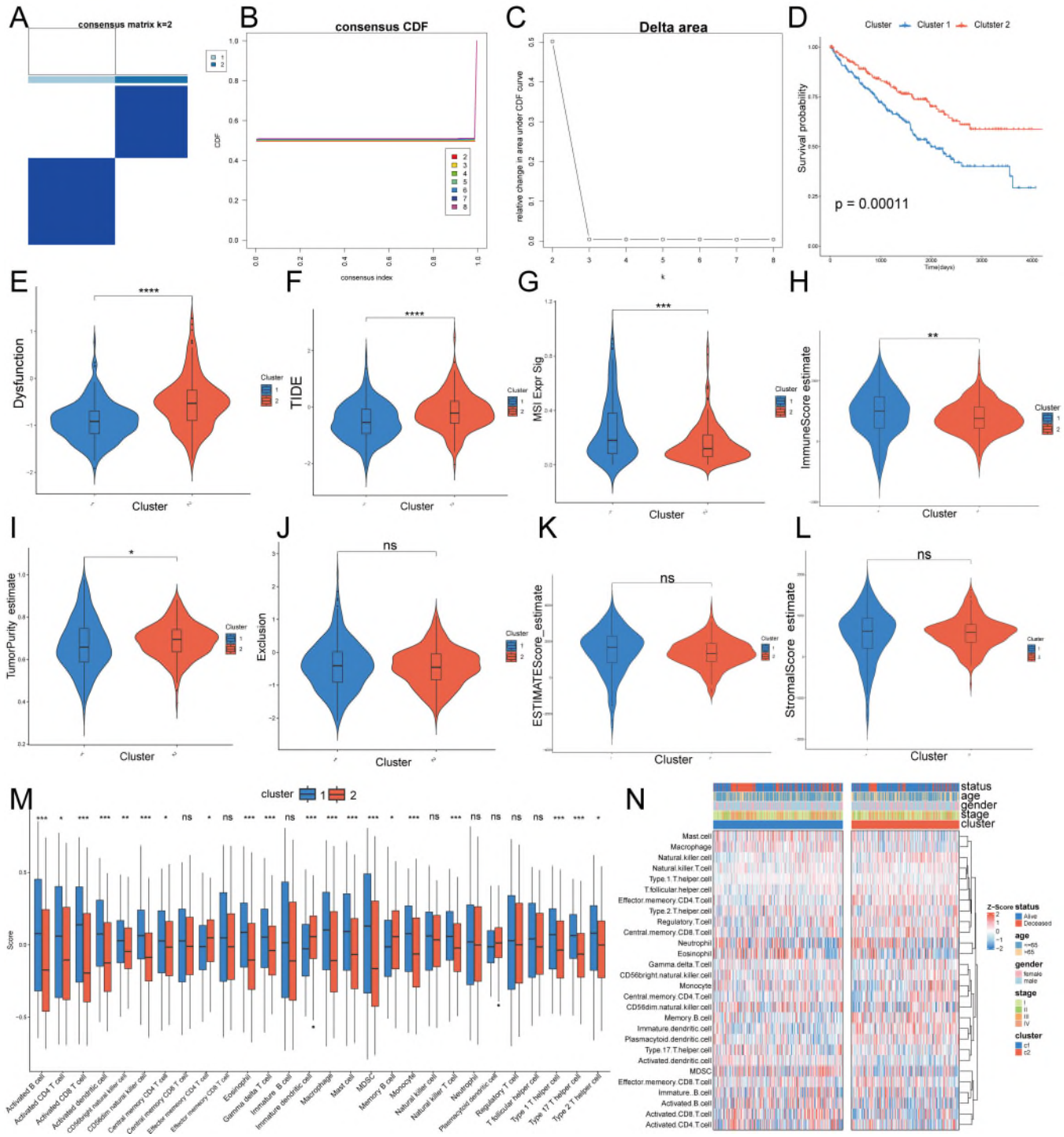


Figure 2. Cancer driver gene-related molecular subgroups. (**A**) Consensus matrix for five core DECDRGs in the TCGA-KIRC cohort at k = 2. (B) CDF curves for different k values. (**C**) Relative change in the CDF area. (**D**) OS curves for C1 and C2 (P = 0.00011). (**E**-**L**) Violin plots comparing T cell dysfunction, TIDE, MSI, immune score, tumor purity, ESTIMATE score, and stromal score

between clusters. ns, not significant; *P < 0.05; **P < 0.01; ***P < 0.001. (M) ssGSEA-based distribution of 28 immune cell subsets. (**N**) Heatmap of ssGSEA immune infiltration with survival status, age, sex, stage, and subgroup annotations.

	C1 (N=279)	C2 (N=232)	Total (N=511)
Survival time (years)			
Mean (SD)	3.45 (2.48)	3.87 (2.75)	3.64 (2.61)
Median [min, max]	3.08 [0.0055, 11.1]	3.64 [0.0082, 12.4]	3.26 [0.0055, 12.4]
Age (years)			
Mean (SD)	59.87 (11.70)	61.56 (12.05)	60.64 (11.88)
Median [min, max]	60.00 [26.0000, 88.0]	61.00 [34.0000, 88.0]	61.00 [26.0000, 88.0]
Gender			
Female	91 (32.6%)	88 (37.9%)	179 (35.0%)
Male	188 (67.4%)	144 (62.1%)	332 (65.0%)
Stage			
I	134 (48.0%)	117 (50.4%)	251 (49.1%)
II	26 (9.3%)	29 (12.5%)	55 (10.8%)
III	66 (23.7%)	56 (24.1%)	122 (23.9%)
IV	53 (19.0%)	30 (12.9%)	83 (16.2%)

Table 1. Baseline clinical features of patients assigned to the C1 and C2 clusters.

Identification of Key Modules and Hub Genes

WGCNA was performed in the TCGA-KIRC training cohort to identify cluster-associated gene modules. A soft-thresholding power of beta = 7 was chosen for approximate scale-free topology (Figure 3A). Thirteen co-expression modules were detected (Figure 3B, E). The MEturquoise module correlated positively with C2 (cor = 0.50, P = 6e-33) and negatively with C1 (cor = -0.50, P = 6e-33) (Figure 3C). Network and adjacency heatmaps supported the module structure (Figure 3D-E). Within the turquoise module, GS and MM were strongly correlated (cor = 0.75, P < 1e-200; Figure 3F). Applying GS > 0.1 and MM > 0.4 identified 2,751 module hub genes. Intersecting these genes with DECDRGs produced 148 key DECDRGs, among which 105 were associated with prognosis in univariate Cox analysis (Figure S3).

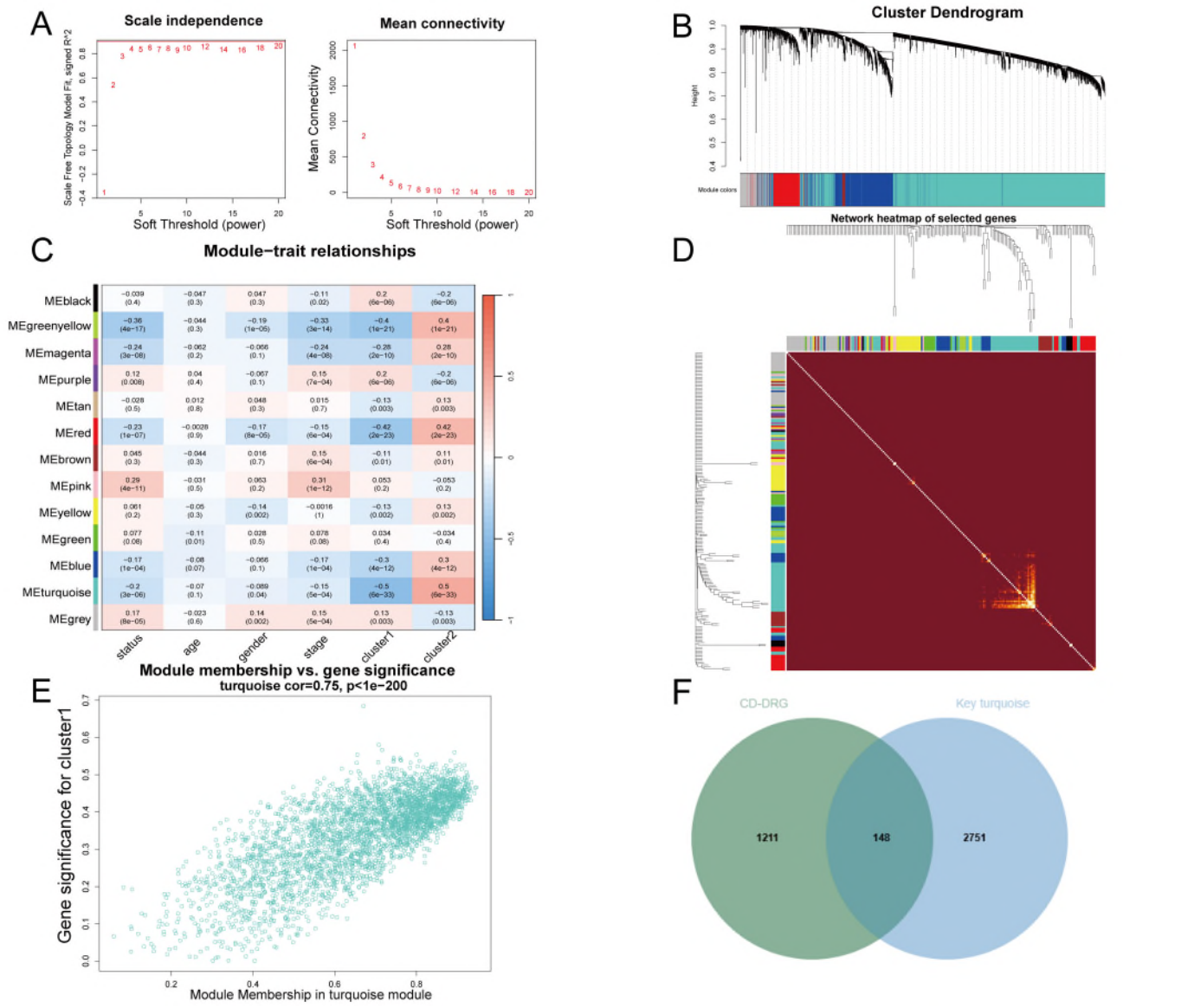


Figure 3. Key WGCNA modules and hub-gene screening. (**A**) Scale-free topology fit and mean connectivity across candidate soft-thresholding powers. (**B**) WGCNA dendrogram with module colors. (**C**) Module-trait correlation heatmap; MEturquoise was most closely related to C2 (cor = 0.50, P = 6e-33). (**D**) Network heatmap for selected genes. (**E**) Module eigengene adjacency heatmap. (F) GS-MM scatter plot in the turquoise module (cor = 0.75, P < 1e-200). The Venn diagram shows 148 DECDRGs shared by the turquoise module and the DECDRG list.

Construction and Validation of the CDPI

Four algorithms, Lasso, decision tree, random forest, and XGBoost, were combined to rank the 105 prognosis-related genes and select the 15 strongest candidates (Figure 4). Multivariate Cox modeling then reduced the set to five genes: PLCL1, GABRB3, USP46, RNF152, and PFKP. CDPI values were calculated from the expression levels of these genes weighted by their regression coefficients.

CDPI = (−0.37709761) × expression(*PLCL1*) + (−0.23607091) × expression(*PFKP*) + (−0.17429854) × expression(*GABRB3*) + (0.34885099) × expression(*USP46*) + (−0.20304284) ×

expression(*RNF152*)

The median CDPI value was used as the cutoff for assigning patients to low- or high-CDPI groups. Baseline clinical characteristics for these groups are listed in Table 2.

Survival analysis showed that the high-CDPI group had worse OS than the low-CDPI group in both TCGA ($P < 0.0001$; Figure 5A) and E-MTAB-1980 ($P < 0.0001$; Figure 5B). A prognostic nomogram incorporating CDPI, age, sex, and stage was built (Figure 5C). Univariate and multivariate Cox models both supported CDPI as an independent survival predictor (Figure 5D, E). Calibration plots showed close agreement between predicted and observed survival at 1, 3, and 5 years (Figure 5F). Compared with CDPI alone and individual clinical variables, the nomogram achieved a higher C-index (Figure 5G), and DCA showed greater net clinical benefit (Figure 5H). These findings indicate that the CDPI nomogram may provide quantitative support for personalized KIRC risk assessment.

In TCGA-KIRC, time-dependent ROC curves produced AUCs of 0.86, 0.83, and 0.78 for 1-, 3-, and 5-year OS, respectively (Figure 6A). In E-MTAB-1980, the corresponding AUCs were 0.74, 0.76, and 0.78 (Figure 6B), indicating stable discrimination across datasets. As CDPI increased, PLCL1, GABRB3, PFKP, and RNF152 showed a gradual shift toward lower expression, visible as a red-to-blue transition on the heatmap. USP46 showed a less uniform pattern, with mild enrichment in the high-CDPI group, consistent with its positive Cox coefficient. The validation cohort showed a comparable distribution (Figure 6C-D).

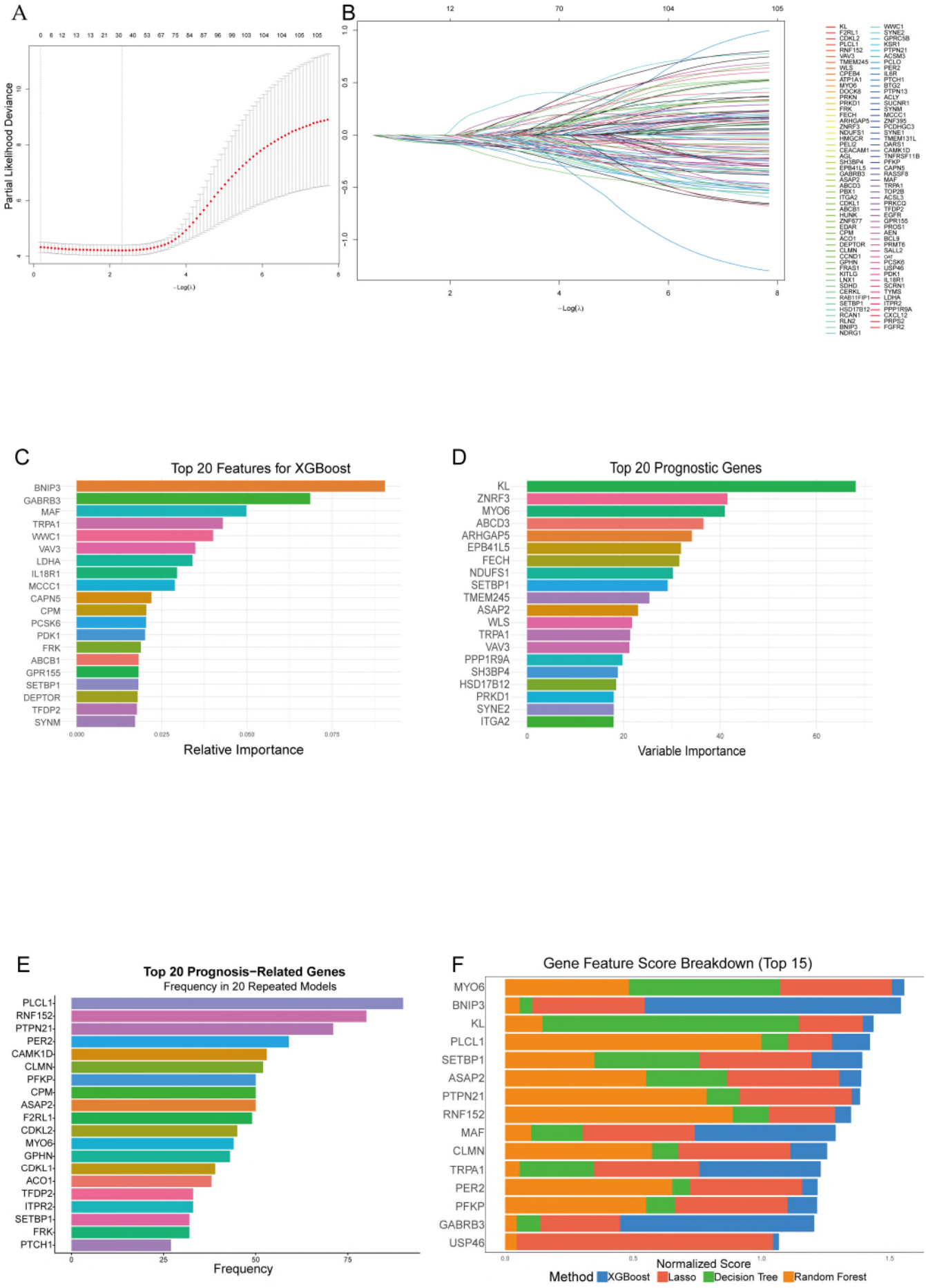


Figure 4. CDPI construction. (**A**) Ten-fold cross-validation for lambda selection in Lasso Cox regression. (**B**) Lasso coefficient trajectories for 105 prognostic DECDRGs. (**C**) XGBoost

importance ranking of the top 20 features. (**D**) Top 20 genes ranked by the decision-tree model. (**E**) Frequency of the top 20 genes across 20 repeated random-forest runs. (**F**) Composite feature-score decomposition for the top 15 genes across the four machine-learning approaches.

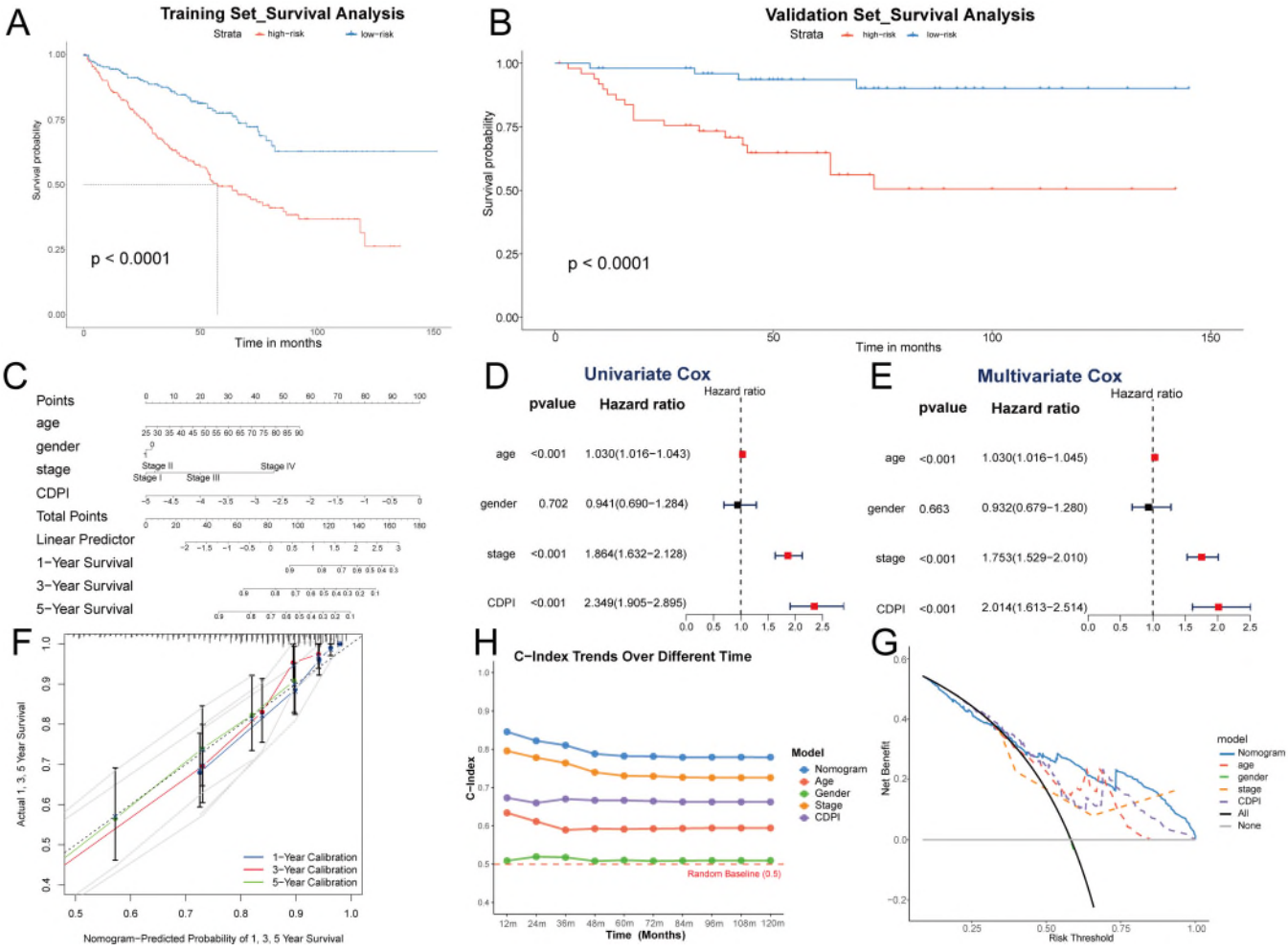


Figure 5. CDPI validation. (**A**) OS comparison between the two CDPI strata in TCGA-KIRC (P < 0.0001). (**B**) OS comparison in E-MTAB-1980 (P < 0.0001). (**C**) Nomogram using CDPI, age, sex, and stage to estimate 1-, 3-, and 5-year OS. (**D**) Univariate Cox forest plot for CDPI and clinical factors. (**E**) Multivariate Cox forest plot showing the independent contribution of CDPI. (**F**) Calibration of predicted OS at 1, 3, and 5 years. (**H**) Time-dependent C-index comparison for the nomogram and individual predictors. (**G**) DCA comparing clinical net benefit among models.

	Low risk (N=256)	High risk (N=255)	Total (N=511)
Survival time (years)			
Mean (SD)	3.82 (2.63)	3.57 (2.68)	3.69 (2.65)
Median [min, max]	3.78 [0.0056, 12.6]	3.05 [0.0444, 11.3]	3.31 [0.0056, 12.6]
Age (years)			
Mean (SD)	60.0 (11.9)	61.2 (11.9)	60.6 (11.9)
Median [min, max]	60.0 [34.0, 88.0]	61.0 [26.0, 86.0]	61.0 [26.0, 88.0]
Gender			
Female	151 (59.0%)	181 (71.0%)	332 (65.0%)
Male	105 (41.0%)	74 (29.0%)	179 (35.0%)
Stage			
I	157 (61.3%)	94 (36.9%)	251 (49.1%)
II	25 (9.8%)	30 (11.8%)	55 (10.8%)
III	53 (20.7%)	69 (27.1%)	122 (23.9%)
IV	21 (8.2%)	62 (24.3%)	83 (16.2%)

Table 2. Clinicopathological features of TCGA patients stratified by CDPI group.

	Low risk (N=51)	High risk (N=50)	Total (N=101)
Survival time (years)			
Mean (SD)	5.36 (2.86)	4.48 (3.00)	4.92 (2.95)
Median [min, max]	4.75 [0.8333, 12.1]	3.83 [0.0833, 11.8]	4.25 [0.0833, 12.1]
Age (years)			
Mean (SD)	64.8 (12.2)	62.1 (10.6)	63.5 (11.5)
Median [min, max]	67.0 [35.0, 91.0]	61.0 [35.0, 82.0]	64.0 [35.0, 91.0]
Gender			
Female	38 (74.5%)	39 (78.0%)	77 (76.2%)
Male	13 (25.5%)	11 (22.0%)	24 (23.8%)
Stage			
I	38 (74.5%)	28 (56.0%)	66 (65.3%)
II	6 (11.8%)	4 (8.0%)	10 (9.9%)
III	4 (7.8%)	9 (18.0%)	13 (12.9%)
IV	3 (5.9%)	9 (18.0%)	12 (11.9%)

Table 3. Clinicopathological features of E-MTAB-1980 patients stratified by CDPI group.

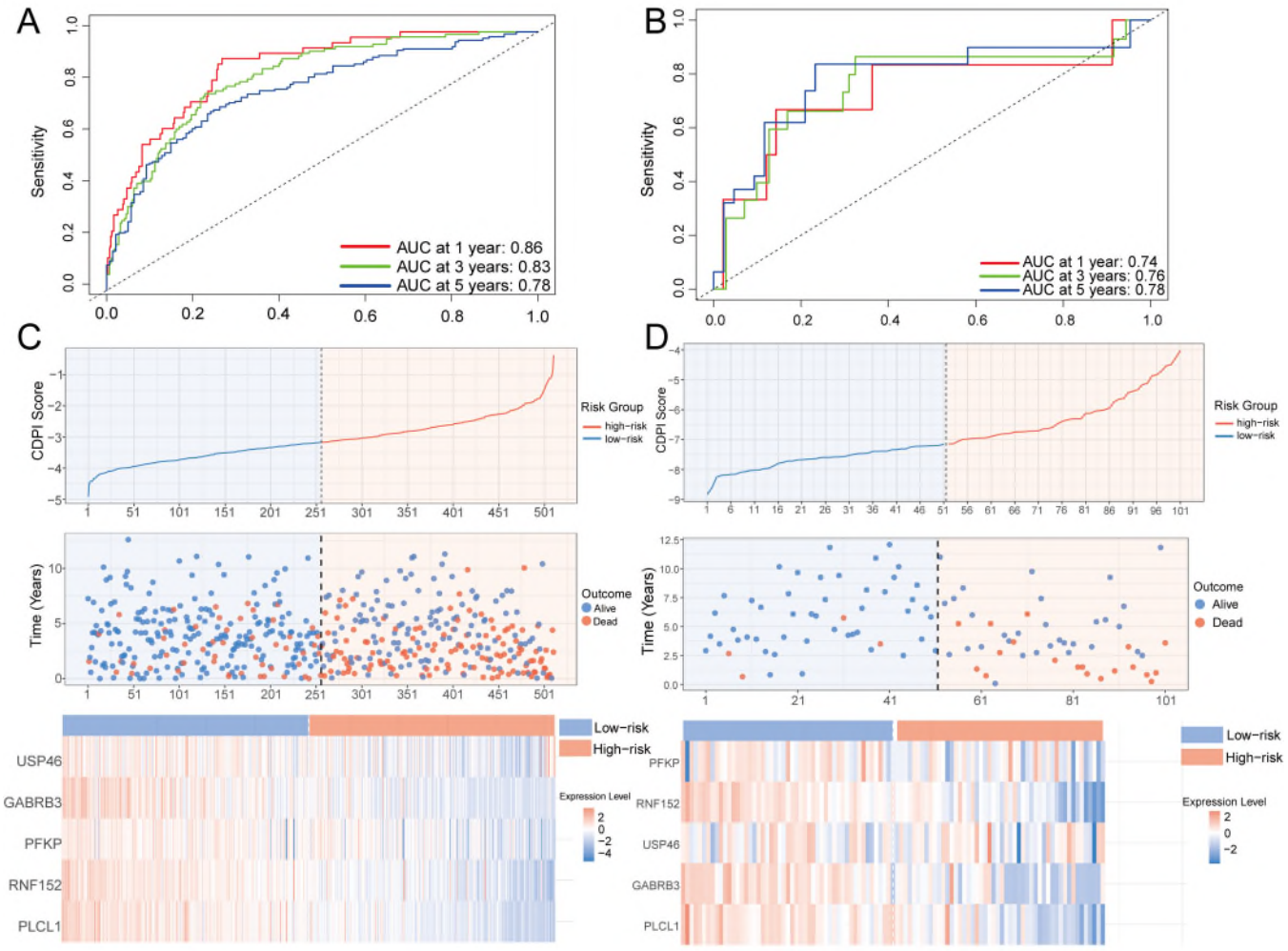


Figure 6. Prognostic performance and CDPI distribution. (**A**) Time-dependent ROC curves for 1-, 3-, and 5-year OS in TCGA-KIRC, with AUCs of 0.86, 0.83, and 0.78. (**B**) ROC curves in E-MTAB-1980. (**C**) CDPI ranking, survival status, and five-gene expression heatmap in TCGA-KIRC. (**D**) Corresponding plots for E-MTAB-1980. The dashed line marks the median CDPI cutoff.

Evaluation of the CDPI's clinical significance

To evaluate whether the CDPI retained prognostic relevance across clinical contexts, patients were grouped by age, sex, pathological stage, and cluster subtype. Higher CDPI values were observed in patients who died, belonged to C1, were classified as high risk, were male, or had stage IV disease (Figure 7A-F). Within sex and age strata, high CDPI consistently predicted poorer survival (all $P < 0.0001$; Figure 7G-J). CDPI also remained unfavorable in stage III-IV disease ($P < 0.0001$), whereas the difference was not significant in stage I-II disease ($P = 0.34$; Figure 7K-L). Because 65% of the validation cohort consisted of stage I cases, the survival advantage of early disease may have weakened CDPI separation. Overall, these results support the clinical utility of CDPI for KIRC prognosis.

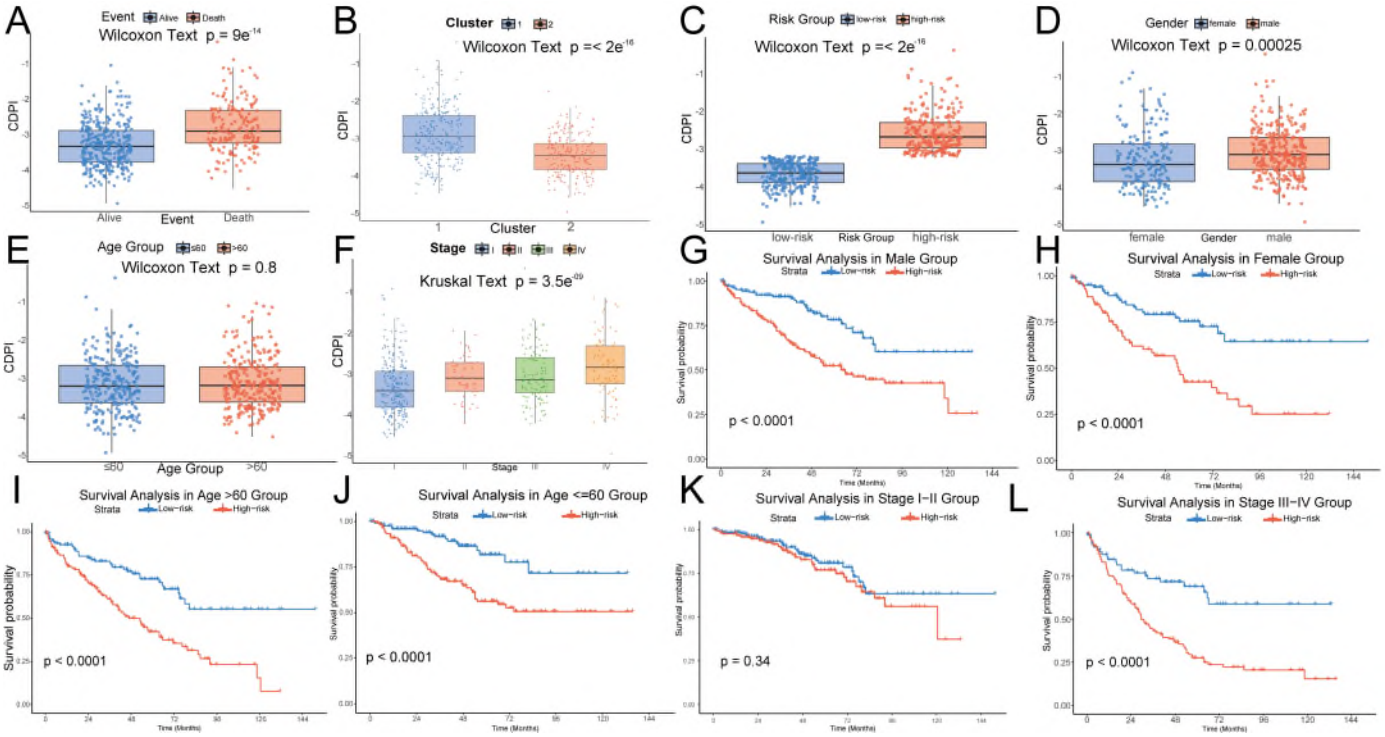


Figure 7. Clinical associations of CDPI. (**A**-**F**) CDPI levels according to survival event, cluster subtype, risk group, sex, age, and stage. (**G**-**L**) Stratified OS analyses comparing high- and low-CDPI patients in male, female, age > 60 years, age <= 60 years, stage I-II, and stage III-IV subgroups. P values were calculated with log-rank tests.

Functional Enrichment Analysis

GSEA was used to investigate biological programs associated with CDPI-defined risk. GO results linked DECDRGs to leukocyte proliferation, inflammatory-response regulation, and leukocyte adhesion (Figure 8A). KEGG analysis emphasized cytokine-cytokine receptor interaction, Th17 cell differentiation, and viral protein interactions with cytokines and cytokine receptors (Figure 8B). Transporter-related GO terms, including sodium ion transmembrane transporter activity and symporter activity, were enriched in the low-CDPI group (Figure 8C). The high-CDPI group instead showed enrichment for leukocyte differentiation, hematopoiesis, and monocyte differentiation (Figure 8D).

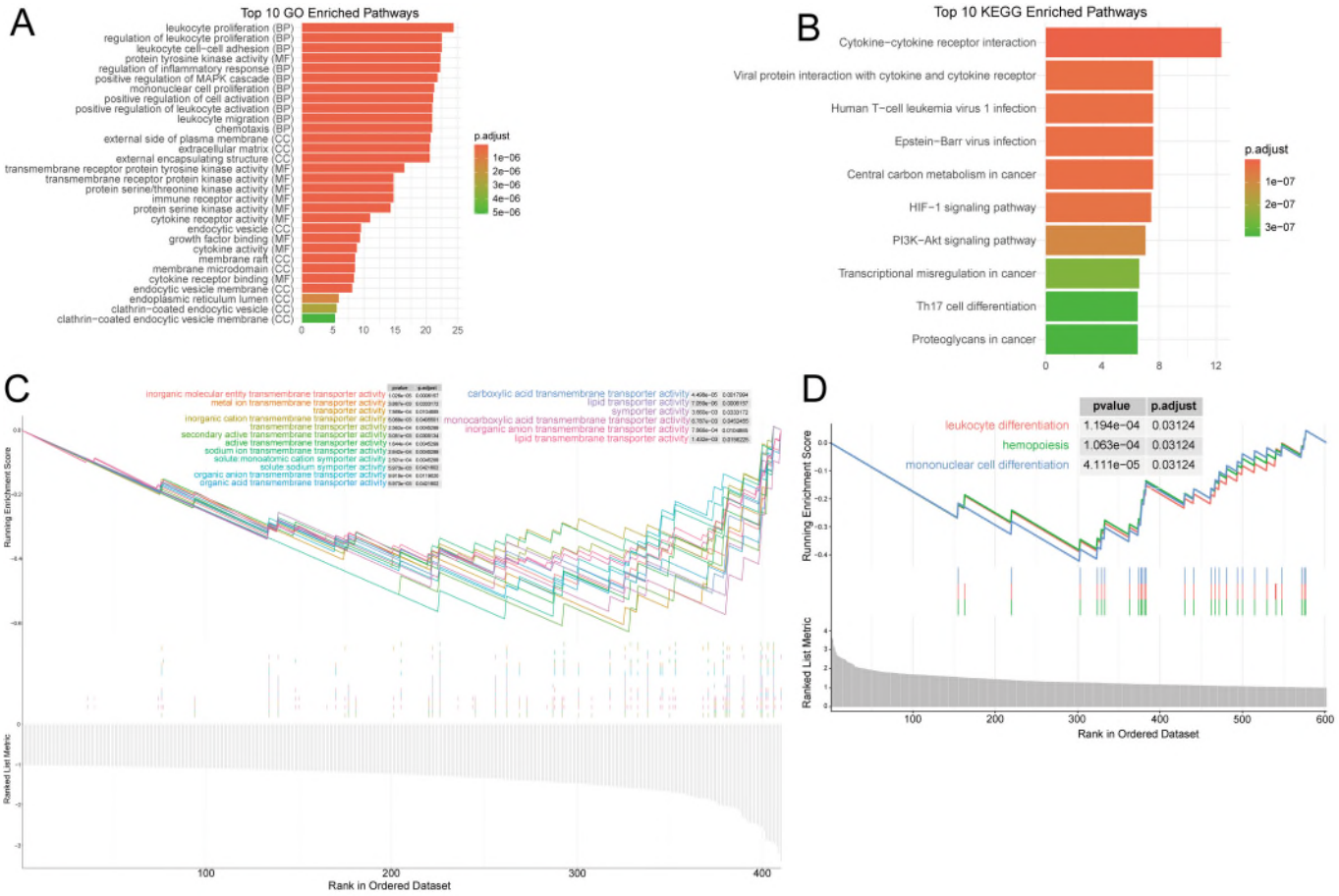


Figure 8. GSEA results. (**A**) Top GO terms across biological process, cellular component, and molecular function categories among DECDRGs. (**B**) Top KEGG pathways among DECDRGs. (**C**) Enrichment curves for transporter activity-related GO terms in the low-CDPI group. (**D**) Enrichment curves for leukocyte differentiation, hematopoiesis, and monocyte differentiation in the high-CDPI group. NES, normalized enrichment score.

Characterization of the Tumor Immune Microenvironment

Immune and stromal features were estimated with nine computational approaches. ESTIMATE showed higher immune and ESTIMATE scores but lower tumor purity in the high-CDPI group, while stromal scores were similar between groups (Figure 9A-D). ssGSEA indicated a broad increase in immune-cell infiltration in high-CDPI tumors (Figure 9E). The five signature genes showed only weak correlations with most infiltrating immune cell types, and significant positive or negative associations were uncommon (Figure 9F). This suggests that the prognostic effect of the CDPI genes may be mediated more by intrinsic tumor biology than by direct control of immune-cell abundance. The ssGSEA findings were checked with MCP-counter, EPIC, xCell, CIBERSORT, quanTIseq, and TIMER to reduce method-specific bias (Figures S6 and S7).

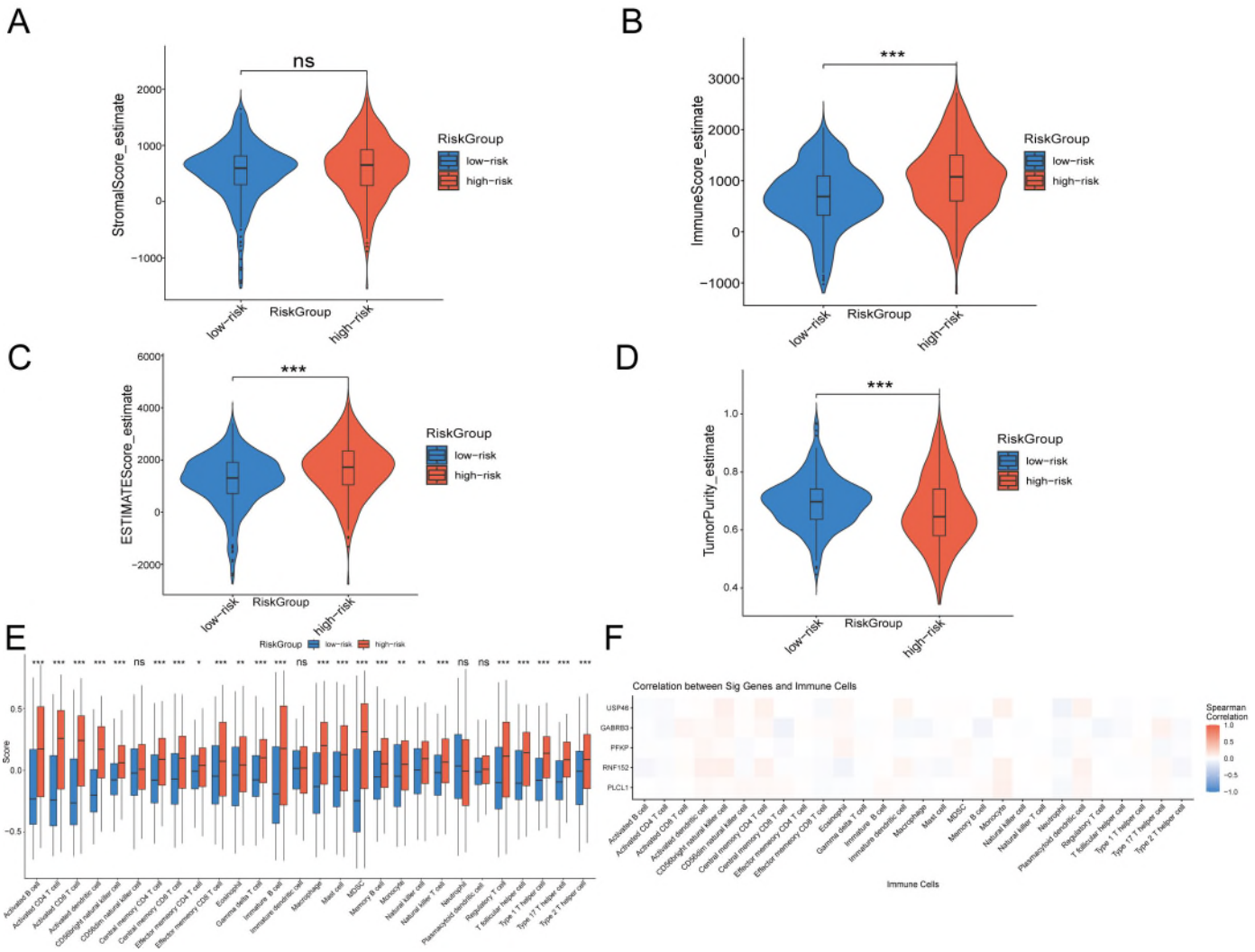


Figure 9. Tumor immune microenvironment analysis. (**A**-**D**) Stromal score, immune score, ESTIMATE score, and tumor purity in high- and low-CDPI tumors. ns, not significant; P < 0.001. (**E**) ssGSEA-based abundance of 28 immune cell subsets in the two groups. (**F**) Spearman correlation heatmap for the five characteristic DECDRGs and tumor-infiltrating immune cell types.

Mutational Landscape Analysis

Mutation profiles differed between CDPI groups, particularly for VHL, PBRM1, TTN, and SETD2 (Figure 10A-B). Most frequently mutated genes tended to co-occur, whereas mutually exclusive pairs were less common. In the high-CDPI group, SETD2-PBRM1 showed significant co-occurrence (Figure 10C). In the low-CDPI group, BAP1-SETD2 was a representative co-occurring pair (Figure 10D). Mutations in the five signature DECDRGs were infrequent and were mainly missense variants (Figure 10E).

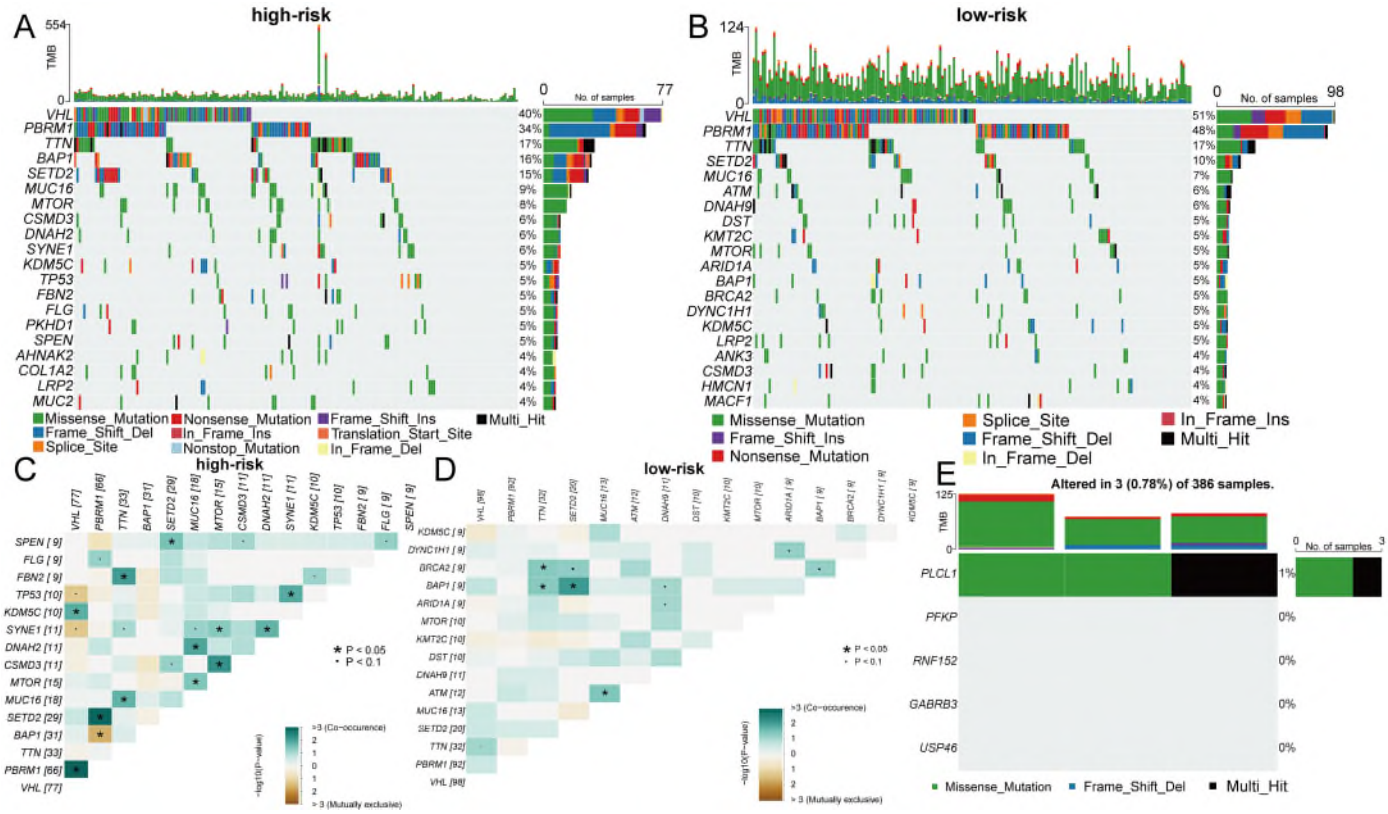


Figure 10. Mutation profiles by CDPI group. (**A**) Waterfall plot for high-CDPI tumors. (**B**) Waterfall plot for low-CDPI tumors. (**C**) Co-occurrence and mutual-exclusivity heatmap for the high-CDPI group. (**D**) Corresponding heatmap for the low-CDPI group. *P < 0.05; dot, P < 0.1. (**E**) Mutation frequency and variant types for the five characteristic DECDRGs.

Assessment of Immunotherapy Effectiveness and Immune Function

Immune checkpoint blockade is clinically beneficial in several tumor types. Here, high-CDPI tumors showed higher TIDE, T cell dysfunction, and T cell exclusion scores, but lower MSI scores, pointing to stronger immune-escape potential (Figure 11A). IPS did not separate the two CDPI groups for most ICI combinations, although several comparisons reached nominal significance (Figure 11B), suggesting that CDPI alone may not be sufficient for predicting ICI efficacy. Pathway-level ssGSEA showed higher activity of type II IFN response, MHC class I, APC co-stimulation, HLA, cytolytic activity, inflammation promotion, T cell co-inhibition, checkpoints, and CCR pathways in the high-CDPI group (Figure 11C). The five signature genes were positively related to many immune checkpoints, and CD276, LAG3, PD-L1, CTLA4, and PD-1 were more highly expressed in high-CDPI tumors (Figure 11D-E).

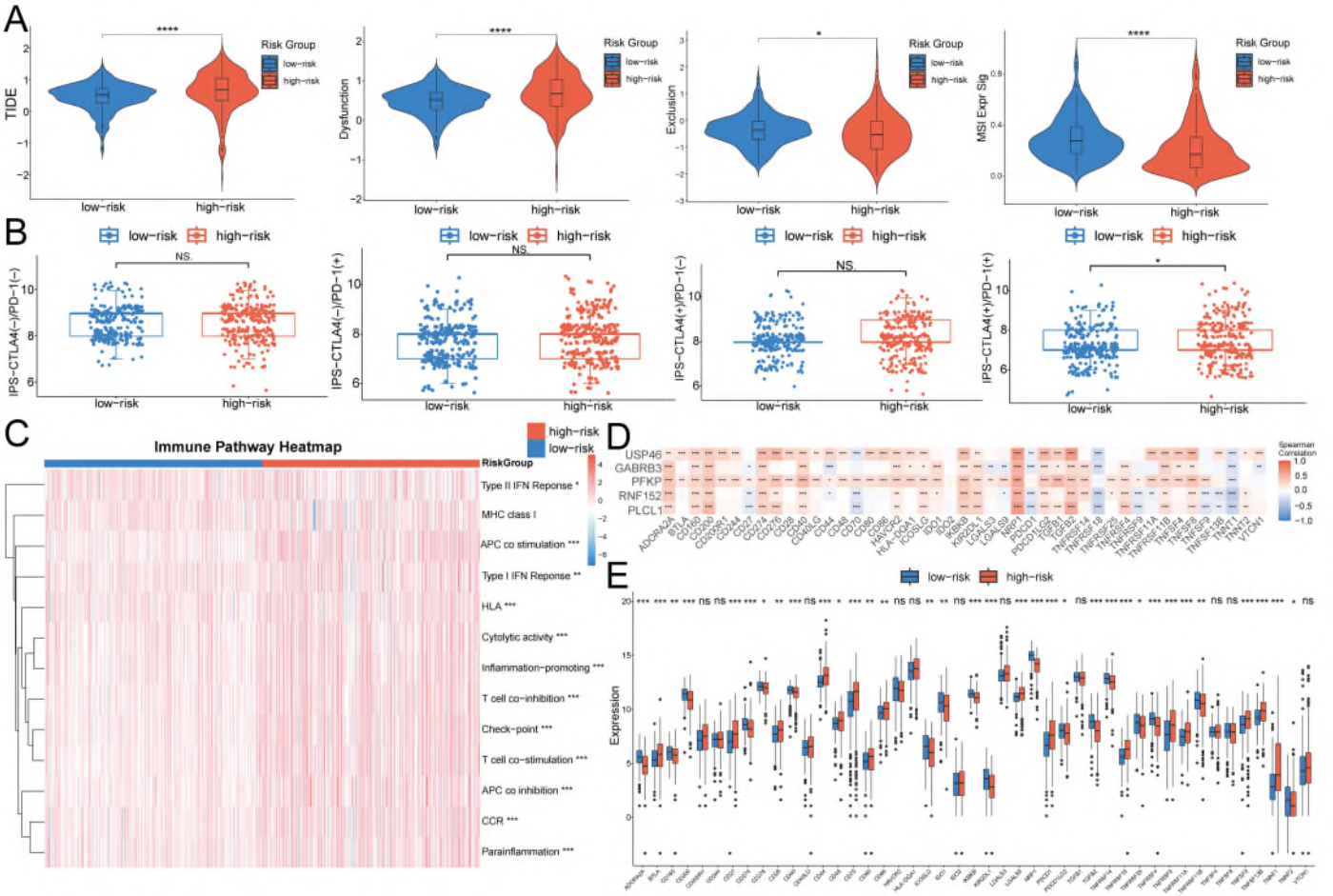


Figure 11. Immunotherapy-related prediction and immune function. (**A**) TIDE, T cell dysfunction, T cell exclusion, and MSI scores across CDPI strata. P < 0.001; P < 0.05. (**B**) IPS comparisons for anti-PD-1 and anti-CTLA-4 treatment combinations. NS, not significant. (**C**) ssGSEA heatmap of immune pathway activity by CDPI group. (**D**) Correlations between the five characteristic DECDRGs and common immune checkpoints. (**E**) Immune checkpoint expression by CDPI category. P < 0.05; *P < 0.01; P < 0.001.

Drug Sensitivity Analysis

Predicted drug-response profiles were compared to explore the treatment implications of CDPI in KIRC. High-CDPI patients had higher predicted IC50 values for Daporinad, osimertinib, and cediranib, indicating lower sensitivity, but lower IC50 values for gemcitabine, epirubicin, docetaxel, and AZD7762, indicating greater sensitivity (Figure 12A). These findings suggest that CDPI may contribute to chemotherapy selection. CellMiner analysis was then used to connect the five signature genes with drug response. Higher RNF152 and PLCL1 expression correlated with sensitivity to multiple drugs, whereas higher USP46, PFKP, and GABRB3 expression correlated with resistance (Figure 12B). CTRP/GDSC analyses further showed positive associations between GABRB3 and PFKP expression and drug sensitivity, while RNF152, PLCL1, and USP46 showed negative associations (Figure 12C).

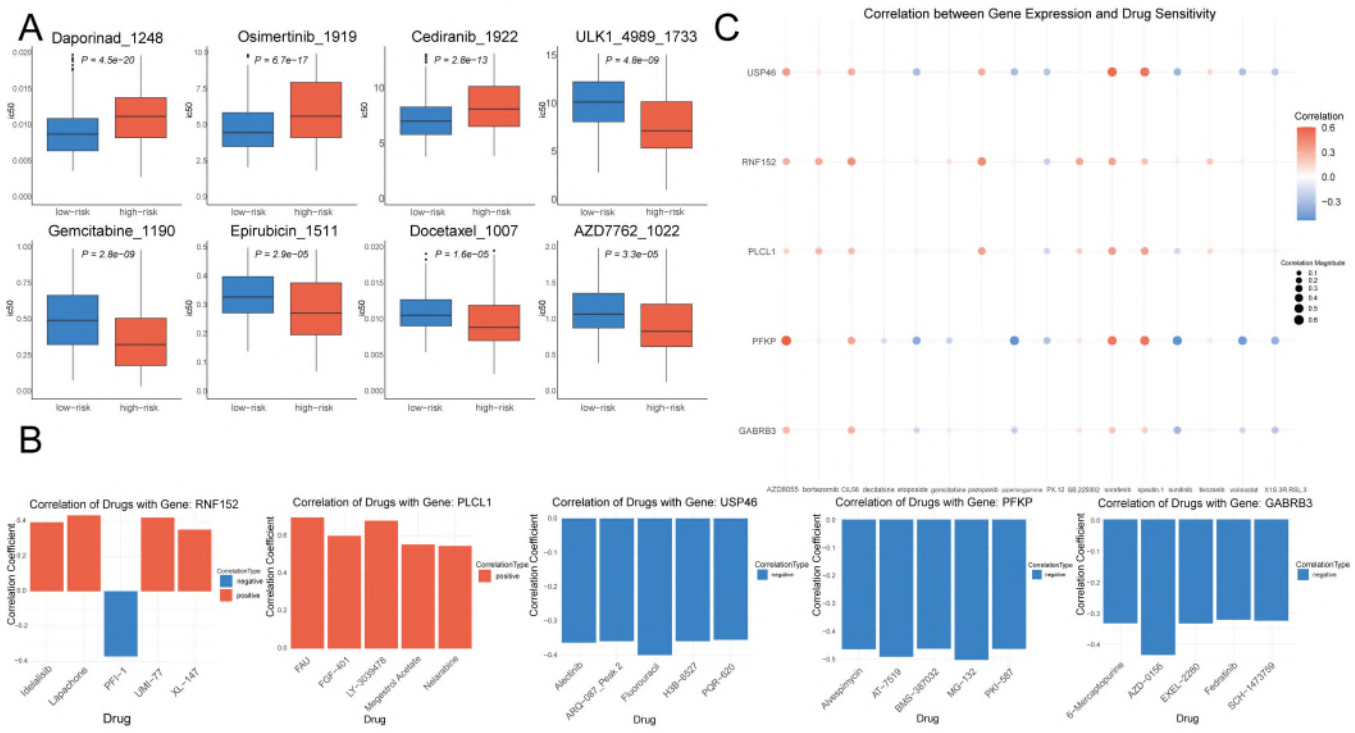


Figure 12. Drug-response analysis by CDPI group. (**A**) Predicted IC50 values for Daporinad, osimertinib, cediranib, ULK1 inhibitor, gemcitabine, epirubicin, docetaxel, and AZD7762 across CDPI strata. (**B**) Correlations between the five characteristic DECDRGs and drug sensitivity, showing the top five drugs for each gene. (**C**) CTRP-based dot plot linking gene expression with drug sensitivity. Dot size indicates correlation magnitude, and color indicates direction.

Discussion

KIRC shows substantial molecular heterogeneity[49], and alterations in driver genes such as VHL, PBRM1, and SETD2 are important for its initiation and progression[6]. Rather than evaluating individual genes in isolation, we developed a composite CDG-based index, the CDPI, incorporating PLCL1, GABRB3, USP46, RNF152, and PFKP. USP46 had a positive coefficient and therefore contributed to risk, whereas the other four genes had negative coefficients. This bidirectional structure may reflect the mixed biological functions of the driver-gene network, in which some nodes support tumor growth through glycolysis, ubiquitination, or ion channel signaling, while others may constrain progression through metabolic or apoptotic pathways.

Starting from dysregulated CDGs, consensus clustering identified two KIRC molecular subtypes with clear survival differences. C1 had poorer OS despite higher tumor purity and greater immune-cell infiltration, a pattern reproduced across six deconvolution methods. This counterintuitive result is compatible with an immune-rich but suppressed tumor microenvironment[50,51]. Exhausted cytotoxic T cells, regulatory T cells, or myeloid-derived suppressor cells may contribute to this pro-tumor immune state despite abundant immune cells[31]. C2 showed better survival and higher TIDE scores but lower infiltration of most immune cell subsets[31], implying that these tumors may evade immune surveillance through intrinsic suppressive programs or mechanisms other than cell exclusion. Similar interactions between genomic alterations and immune context have been

described in renal cancer[52,52]. The stable k = 2 structure therefore provides a CDG-centered stratification that complements existing ccA/ccB classifications.

By combining WGCNA with four machine-learning methods, we constructed a five-gene CDPI with independent prognostic value. The consensus modeling strategy helped reduce dependence on any single algorithm and improved the robustness of the selected signature. Lower PLCL1, PFKP, GABRB3, and RNF152 expression in high-risk patients suggests possible tumor-suppressive roles. PFKP, for example, is a glycolytic enzyme; its reduced expression may reflect metabolic remodeling related to HIF stabilization in KIRC[53], although its prognostic connection through metabolic vulnerability remains to be defined. In contrast, increased USP46 expression in high-risk tumors implicates dysregulated protein stability control[54]. Validation in two cohorts supports CDPI as an independent risk marker beyond conventional clinicopathological variables.

CDPI was also closely connected with immune microenvironment features. High CDPI scores were associated with higher immune and ESTIMATE scores, lower tumor purity, and increased TIDE, dysfunction, and exclusion scores. These findings describe an immune-rich state that is nevertheless functionally impaired and does not provide a survival advantage[31,51]. The higher expression of PD-L1, CTLA-4, and LAG3 in high-CDPI tumors is consistent with checkpoint activation in dysfunctional immune contexts[51]. Correlations between these checkpoints and CDPI genes suggest that the signature may mark a tumor program that attracts immune cells while simultaneously promoting suppressive counter-regulation[52]. This provides a possible explanation for the immune-escape phenotype and supports further evaluation of CDPI as a biomarker for immune checkpoint blockade response. The convergence of nine immune-infiltration algorithms strengthens this interpretation.

The predicted drug-response results suggest additional clinical relevance. High-CDPI tumors were more sensitive to agents such as gemcitabine and docetaxel but more resistant to cediranib[9]. These differences may be related to the biology of the signature genes. Reduced PFKP expression in high-risk tumors could indicate a metabolic state that creates vulnerability to selected cytotoxic drugs, consistent with the role of metabolic reprogramming in treatment response[53]. Higher RNF152 and PLCL1 expression, in contrast, may contribute to multidrug resistance through effects on pro-survival proteins or drug-efflux pathways, a possibility that requires experimental testing. Because these predictions were generated from resources such as GDSC, they should be interpreted as hypothesis-generating evidence[55]. Patient-derived experimental models will be needed to determine whether the predicted sensitivities translate into actual treatment responses[56].

The enriched pathways, including PI3K-Akt and HIF-1 signaling, provide a broader biological context for the hub DECDRGs, while the final CDPI condenses this information into five genes with independent survival relevance. EGFR, MYC, and GAPDH may connect the driver-gene program to PI3K-Akt and HIF-1 signaling, thereby offering a mechanistic link to KIRC pathogenesis[57,58]. EGFR and MYC are well-established proliferation and survival drivers and may cooperate with the VHL-HIF axis in KIRC[58,59]. GAPDH, beyond its glycolytic housekeeping role, is a HIF target and participates in metabolic rewiring in KIRC[53]. The PI3K-Akt enrichment

also emphasizes growth factor and nutrient-sensing pathways that interact with hypoxic signaling to support survival and apoptosis resistance[57]. These convergent pathways indicate that KIRC progression is shaped by coordinated driver networks rather than isolated genetic events[58].

Limitations

Several limitations should be noted. First, the model and mechanistic inferences were derived from retrospective public transcriptomic datasets, mainly TCGA and ArrayExpress, and may therefore be influenced by selection bias or batch effects. Independent prospective cohorts, particularly cohorts including diverse ethnic populations such as Asian patients, are needed to test generalizability. Second, the study lacks functional validation, so the roles of USP46 in immune escape and RNF152 in drug resistance remain correlative. In vitro and in vivo perturbation experiments are required to establish causality. In addition, TIDE provides an indirect estimate of immunotherapy response because paired pre- and post-treatment samples from ICI-treated patients were not available. These limitations mean that experimental and clinical validation is necessary before clinical translation.

Conclusion

This study established a CDG-based CDPI that independently predicts KIRC prognosis while integrating driver-gene expression, immune context, and predicted drug response. The index offers a quantitative basis for risk assessment and treatment exploration, but prospective validation remains essential.

Funding

This work was supported by grants from Guilin Science Research and Technology Development Project (20220139-13-2), Guangxi Key Laboratory of Tumor Immunology and Microenvironmental Regulation (2023KF006, 3030302213).

Ethics, Consent to Participate, and Consent to Publish declarations

Not applicable. This study utilized publicly available datasets (TCGA and ArrayExpress) and did not involve human participants, human tissue, or animal experiments.

Author Contributions

F.T. conceived and designed the study, performed the bioinformatics analysis, generated all figures, and wrote the original draft. B.Z. provided technical guidance on R programming. S.L. and X.H. supervised the study and revised the manuscript. All authors reviewed and approved the final version.

Conflicts of Interest

The authors declare no conflicts of interest.

1. Bukavina, L., Bensalah, K., Bray, F., Carlo, M., Challacombe, B., Karam, J.A., Kassouf, W., Mitchell, T., Montironi, R., O'Brien, T., Panebianco, V., Scelo, G., Shuch, B., Van Poppel, H., Blosser, C.D., Psutka, S.P.: Epidemiology of Renal Cell Carcinoma: 2022 Update. European Urology. 82, 529–542 (2022). https://doi.org/10.1016/j.eururo.2022.08.019.
2. Linehan, W.M.: Genetic basis of kidney cancer: Role of genomics for the development of disease-based therapeutics. Genome Res. 22, 2089–2100 (2012). https://doi.org/10.1101/gr.131110.111.
3. Choueiri, T.K., Motzer, R.J.: Systemic Therapy for Metastatic Renal-Cell Carcinoma. N Engl J Med. 376, 354–366 (2017). https://doi.org/10.1056/NEJMra1601333.
4. Hsieh, J.J., Purdue, M.P., Signoretti, S., Swanton, C., Albiges, L., Schmidinger, M., Heng, D.Y., Larkin, J., Ficarra, V.: Renal cell carcinoma. Nat Rev Dis Primers. 3, 17009 (2017). https://doi.org/10.1038/nrdp.2017.9.
5. Hanahan, D., Weinberg, R.A.: Hallmarks of Cancer: The Next Generation. Cell. 144, 646–674 (2011). https://doi.org/10.1016/j.cell.2011.02.013.
6. The Cancer Genome Atlas Research Network: Comprehensive molecular characterization of clear cell renal cell carcinoma. Nature. 499, 43–49 (2013). https://doi.org/10.1038/nature12222.
7. Semenza, G.L.: HIF-1 mediates metabolic responses to intratumoral hypoxia and oncogenic mutations. J. Clin. Invest. 123, 3664–3671 (2013). https://doi.org/10.1172/JCI67230.
8. Wolf, M.M., Madden, M.Z., Arner, E.N., Bader, J.E., Ye, X., Vlach, L., Tigue, M.L., Landis, M.D., Jonker, P.B., Hatem, Z., Steiner, K.K., Gaines, D.K., Reinfeld, B.I., Hathaway, E.S., Xin, F., Tantawy, M.N., Haake, S.M., Jonasch, E., Muir, A., Weiss, V.L., Beckermann, K.E., Rathmell, W.K., Rathmell, J.C.: VHL loss reprograms the immune landscape to promote an inflammatory myeloid microenvironment in renal tumorigenesis. Journal of Clinical Investigation. 134, e173934 (2024). https://doi.org/10.1172/JCI173934.
9. Miao, D., Margolis, C.A., Gao, W., Voss, M.H., Li, W., Martini, D.J., Norton, C., Bossé, D., Wankowicz, S.M., Cullen, D., Horak, C., Wind-Rotolo, M., Tracy, A., Giannakis, M., Hodi, F.S., Drake, C.G., Ball, M.W., Allaf, M.E., Snyder, A., Hellmann, M.D., Ho, T., Motzer, R.J., Signoretti, S., Kaelin, W.G., Choueiri, T.K., Van Allen, E.M.: Genomic correlates of response to immune checkpoint therapies in clear cell renal cell carcinoma. Science. 359, 801–806 (2018). https://doi.org/10.1126/science.aan5951.
10. Kolesnikov, N., Hastings, E., Keays, M., Melnichuk, O., Tang, Y.A., Williams, E., Dylag, M., Kurbatova, N., Brandizi, M., Burdett, T., Megy, K., Pilicheva, E., Rustici, G., Tikhonov, A., Parkinson, H., Petryszak, R., Sarkans, U., Brazma, A.: ArrayExpress update—simplifying data submissions. Nucleic Acids Research. 43, D1113–D1116 (2015). https://doi.org/10.1093/nar/gku1057.
11. Safran, M., Dalah, I., Alexander, J., Rosen, N., Iny Stein, T., Shmoish, M., Nativ, N., Bahir, I., Doniger, T., Krug, H., Sirota-Madi, A., Olender, T., Golan, Y., Stelzer, G., Harel, A., Lancet, D.: GeneCards Version 3: the human gene integrator. Database. 2010, baq020–baq020 (2010). https://doi.org/10.1093/database/baq020.
12. Ritchie, M.E., Phipson, B., Wu, D., Hu, Y., Law, C.W., Shi, W., Smyth, G.K.: limma powers

differential expression analyses for RNA-sequencing and microarray studies. Nucleic Acids Research. 43, e47–e47 (2015). https://doi.org/10.1093/nar/gkv007.
13. Szklarczyk, D., Gable, A.L., Lyon, D., Junge, A., Wyder, S., Huerta-Cepas, J., Simonovic, M., Doncheva, N.T., Morris, J.H., Bork, P., Jensen, L.J., Mering, C. von: STRING v11: protein–protein association networks with increased coverage, supporting functional discovery in genome-wide experimental datasets. Nucleic Acids Research. 47, D607–D613 (2019). https://doi.org/10.1093/nar/gky1131.
14. Shannon, P., Markiel, A., Ozier, O., Baliga, N.S., Wang, J.T., Ramage, D., Amin, N., Schwikowski, B., Ideker, T.: Cytoscape: A Software Environment for Integrated Models of Biomolecular Interaction Networks. Genome Res. 13, 2498–2504 (2003). https://doi.org/10.1101/gr.1239303.
15. Bader, G.D., Hogue, C.W.: An automated method for finding molecular complexes in large protein interaction networks. BMC Bioinformatics. 4, 2 (2003). https://doi.org/10.1186/1471-2105-4-2.
16. Chin, C.-H., Chen, S.-H., Wu, H.-H., Ho, C.-W., Ko, M.-T., Lin, C.-Y.: cytoHubba: identifying hub objects and sub-networks from complex interactome. BMC Syst Biol. 8, S11 (2014). https://doi.org/10.1186/1752-0509-8-S4-S11.
17. Zhou, G., Soufan, O., Ewald, J., Hancock, R.E.W., Basu, N., Xia, J.: NetworkAnalyst 3.0: a visual analytics platform for comprehensive gene expression profiling and meta-analysis. Nucleic Acids Research. 47, W234–W241 (2019). https://doi.org/10.1093/nar/gkz240.
18. Fornes, O., Castro-Mondragon, J.A., Khan, A., van der Lee, R., Zhang, X., Richmond, P.A., Modi, B.P., Correard, S., Gheorghe, M., Baranašić, D., Santana-Garcia, W., Tan, G., Chèneby, J., Ballester, B., Parcy, F., Sandelin, A., Lenhard, B., Wasserman, W.W., Mathelier, A.: JASPAR 2020: update of the open-access database of transcription factor binding profiles. Nucleic Acids Research. gkz1001 (2019). https://doi.org/10.1093/nar/gkz1001.
19. Ashburner, M., Ball, C.A., Blake, J.A., Botstein, D., Butler, H., Cherry, J.M., Davis, A.P., Dolinski, K., Dwight, S.S., Eppig, J.T., Harris, M.A., Hill, D.P., Issel-Tarver, L., Kasarskis, A., Lewis, S., Matese, J.C., Richardson, J.E., Ringwald, M., Rubin, G.M., Sherlock, G.: Gene Ontology: tool for the unification of biology. Nat Genet. 25, 25–29 (2000). https://doi.org/10.1038/75556.
20. Kanehisa, M., Goto, S.: KEGG: Kyoto Encyclopedia of Genes and Genomes.
21. Zeng, D., Ye, Z., Shen, R., Yu, G., Wu, J., Xiong, Y., Zhou, R., Qiu, W., Huang, N., Sun, L., Li, X., Bin, J., Liao, Y., Shi, M., Liao, W.: IOBR: Multi-Omics Immuno-Oncology Biological Research to Decode Tumor Microenvironment and Signatures. Front. Immunol. 12, 687975 (2021). https://doi.org/10.3389/fimmu.2021.687975.
22. Becht, E., Giraldo, N.A., Lacroix, L., Buttard, B., Elarouci, N., Petitprez, F., Selves, J., Laurent-Puig, P., Sautès-Fridman, C., Fridman, W.H., De Reyniès, A.: Estimating the population abundance of tissue-infiltrating immune and stromal cell populations using gene expression. Genome Biol. 17, 218 (2016). https://doi.org/10.1186/s13059-016-1070-5.
23. Racle, J., De Jonge, K., Baumgaertner, P., Speiser, D.E., Gfeller, D.: Simultaneous enumeration of cancer and immune cell types from bulk tumor gene expression data. eLife. 6, e26476 (2017). https://doi.org/10.7554/eLife.26476.
24. Aran, D., Hu, Z., Butte, A.J.: xCell: digitally portraying the tissue cellular heterogeneity landscape. Genome Biol. 18, 220 (2017). https://doi.org/10.1186/s13059-017-1349-1.
25. Newman, A.M., Liu, C.L., Green, M.R., Gentles, A.J., Feng, W., Xu, Y., Hoang, C.D., Diehn, M., Alizadeh, A.A.: Robust enumeration of cell subsets from tissue expression profiles. Nat Methods. 12, 453–457 (2015). https://doi.org/10.1038/nmeth.3337.
26. Charoentong, P., Finotello, F., Angelova, M., Mayer, C., Efremova, M., Rieder, D., Hackl, H., Trajanoski, Z.: Pan-cancer Immunogenomic Analyses Reveal Genotype-Immunophenotype

Relationships and Predictors of Response to Checkpoint Blockade. Cell Reports. 18, 248–262 (2017). https://doi.org/10.1016/j.celrep.2016.12.019.
27. Finotello, F., Mayer, C., Plattner, C., Laschober, G., Rieder, D., Hackl, H., Krogsdam, A., Loncova, Z., Posch, W., Wilflingseder, D., Sopper, S., Ijsselsteijn, M., Brouwer, T.P., Johnson, D., Xu, Y., Wang, Y., Sanders, M.E., Estrada, M.V., Ericsson-Gonzalez, P., Charoentong, P., Balko, J., De Miranda, N.F.D.C.C., Trajanoski, Z.: Molecular and pharmacological modulators of the tumor immune contexture revealed by deconvolution of RNA-seq data. Genome Med. 11, 34 (2019). https://doi.org/10.1186/s13073-019-0638-6.
28. Yoshihara, K., Shahmoradgoli, M., Martínez, E., Vegesna, R., Kim, H., Torres-Garcia, W., Treviño, V., Shen, H., Laird, P.W., Levine, D.A., Carter, S.L., Getz, G., Stemke-Hale, K., Mills, G.B., Verhaak, R.G.W.: Inferring tumour purity and stromal and immune cell admixture from expression data. Nat Commun. 4, 2612 (2013). https://doi.org/10.1038/ncomms3612.
29. Li, T., Fan, J., Wang, B., Traugh, N., Chen, Q., Liu, J.S., Li, B., Liu, X.S.: TIMER: A Web Server for Comprehensive Analysis of Tumor-Infiltrating Immune Cells. Cancer Research. 77, e108–e110 (2017). https://doi.org/10.1158/0008-5472.CAN-17-0307.
30. Barbie, D.A., Tamayo, P., Boehm, J.S., Kim, S.Y., Moody, S.E., Dunn, I.F., Schinzel, A.C., Sandy, P., Meylan, E., Scholl, C., Fröhling, S., Chan, E.M., Sos, M.L., Michel, K., Mermel, C., Silver, S.J., Weir, B.A., Reiling, J.H., Sheng, Q., Gupta, P.B., Wadlow, R.C., Le, H., Hoersch, S., Wittner, B.S., Ramaswamy, S., Livingston, D.M., Sabatini, D.M., Meyerson, M., Thomas, R.K., Lander, E.S., Mesirov, J.P., Root, D.E., Gilliland, D.G., Jacks, T., Hahn, W.C.: Systematic RNA interference reveals that oncogenic KRAS-driven cancers require TBK1. Nature. 462, 108–112 (2009). https://doi.org/10.1038/nature08460.
31. Jiang, P., Gu, S., Pan, D., Fu, J., Sahu, A., Hu, X., Li, Z., Traugh, N., Bu, X., Li, B., Liu, J., Freeman, G.J., Brown, M.A., Wucherpfennig, K.W., Liu, X.S.: Signatures of T cell dysfunction and exclusion predict cancer immunotherapy response. Nat Med. 24, 1550–1558 (2018). https://doi.org/10.1038/s41591-018-0136-1.
32. Wilkerson, M.D., Hayes, D.N.: ConsensusClusterPlus: a class discovery tool with confidence assessments and item tracking. Bioinformatics. 26, 1572–1573 (2010). https://doi.org/10.1093/bioinformatics/btq170.
33. Zhang, B., Horvath, S.: A General Framework for Weighted Gene Co-Expression Network Analysis. Statistical Applications in Genetics and Molecular Biology. 4, (2005). https://doi.org/10.2202/1544-6115.1128.
34. Langfelder, P., Horvath, S.: WGCNA: an R package for weighted correlation network analysis. BMC Bioinformatics. 9, 559 (2008). https://doi.org/10.1186/1471-2105-9-559.
35. Simon, N., Friedman, J., Hastie, T., Tibshirani, R.: Regularization Paths for Cox's Proportional Hazards Model via Coordinate Descent. J. Stat. Soft. 39, (2011). https://doi.org/10.18637/jss.v039.i05.
36. López, V., Fernández, A., García, S., Palade, V., Herrera, F.: An insight into classification with imbalanced data: Empirical results and current trends on using data intrinsic characteristics. Information Sciences. 250, 113–141 (2013). https://doi.org/10.1016/j.ins.2013.07.007.
37. Petralia, F., Wang, P., Yang, J., Tu, Z.: Integrative random forest for gene regulatory network inference. Bioinformatics. 31, i197–i205 (2015). https://doi.org/10.1093/bioinformatics/btv268.
38. Therneau, A.E., Atkinson, E.J., Foundation, M.: An Introduction to Recursive Partitioning Using the RPART Routines. Mayo Foundation, Rochester, MN, USA (1997).
39. Prentice, R.L., Zhao, S.: Regression Models and Multivariate Life Tables. Journal of the American Statistical Association. 116, 1330–1345 (2021). https://doi.org/10.1080/01621459.2020.1713792.
40. Blanche, P., Dartigues, J., Jacqmin-Gadda, H.: Estimating and comparing time-dependent areas under receiver operating characteristic curves for censored event times with competing

risks. Statistics in Medicine. 32, 5381–5397 (2013). https://doi.org/10.1002/sim.5958.
41. Vickers, A.J., Elkin, E.B.: Decision Curve Analysis: A Novel Method for Evaluating Prediction Models. Med Decis Making. 26, 565–574 (2006). https://doi.org/10.1177/0272989X06295361.
42. Wu, T., Hu, E., Xu, S., Chen, M., Guo, P., Dai, Z., Feng, T., Zhou, L., Tang, W., Zhan, L., Fu, X., Liu, S., Bo, X., Yu, G.: clusterProfiler 4.0: A universal enrichment tool for interpreting omics data. The Innovation. 2, 100141 (2021). https://doi.org/10.1016/j.xinn.2021.100141.
43. Maeser, D., Gruener, R.F., Huang, R.S.: oncoPredict: an R package for predicting *in vivo* or cancer patient drug response and biomarkers from cell line screening data. Briefings in Bioinformatics. 22, bbab260 (2021). https://doi.org/10.1093/bib/bbab260.
44. Liu, C.-J., Hu, F.-F., Xia, M., Han, L., Zhang, Q., Guo, Y.: GSCALite: A Web Server for Gene Set Cancer Analysis.
45. Colaprico, A., Silva, T.C., Olsen, C., Garofano, L., Cava, C., Garolini, D., Sabedot, T.S., Malta, T.M., Pagnotta, S.M., Castiglioni, I., Ceccarelli, M., Bontempi, G., Noushmehr, H.: TCGAbiolinks: an R/Bioconductor package for integrative analysis of TCGA data. Nucleic Acids Research. 44, e71–e71 (2016). https://doi.org/10.1093/nar/gkv1507.
46. Mayakonda, A., Lin, D.-C., Assenov, Y., Plass, C., Koeffler, H.P.: Maftools: efficient and comprehensive analysis of somatic variants in cancer. Genome Res. 28, 1747–1756 (2018). https://doi.org/10.1101/gr.239244.118.
47. Pontén, F., Jirström, K., Uhlen, M.: The Human Protein Atlas—a tool for pathology. The Journal of Pathology. 216, 387–393 (2008). https://doi.org/10.1002/path.2440.
48. Thul, P.J., Lindskog, C.: The human protein atlas: A spatial map of the human proteome. Protein Science. 27, 233–244 (2018). https://doi.org/10.1002/pro.3307.
49. Gerlinger, M., Rowan, A.J., Horswell, S., Larkin, J., Endesfelder, D., Gronroos, E., Martinez, P., Matthews, N., Stewart, A., Tarpey, P., Varela, I., Phillimore, B., Begum, S., McDonald, N.Q., Butler, A., Jones, D., Raine, K., Latimer, C., Santos, C.R., Nohadani, M., Eklund, A.C., Spencer-Dene, B., Clark, G., Pickering, L., Stamp, G., Gore, M., Szallasi, Z., Downward, J., Futreal, P.A., Swanton, C.: Intratumor Heterogeneity and Branched Evolution Revealed by Multiregion Sequencing. N Engl J Med. 366, 883–892 (2012). https://doi.org/10.1056/NEJMoa1113205.
50. Wherry, E.J., Ha, S.-J., Kaech, S.M., Haining, W.N., Sarkar, S., Kalia, V., Subramaniam, S., Blattman, J.N., Barber, D.L., Ahmed, R.: Molecular Signature of CD8+ T Cell Exhaustion during Chronic Viral Infection. Immunity. 27, 670–684 (2007). https://doi.org/10.1016/j.immuni.2007.09.006.
51. Wherry, E.J., Kurachi, M.: Molecular and cellular insights into T cell exhaustion. Nat Rev Immunol. 15, 486–499 (2015). https://doi.org/10.1038/nri3862.
52. Braun, D.A., Hou, Y., Bakouny, Z., Ficial, M., Sant' Angelo, M., Forman, J., Ross-Macdonald, P., Berger, A.C., Jegede, O.A., Elagina, L., Steinharter, J., Sun, M., Wind-Rotolo, M., Pignon, J.-C., Cherniack, A.D., Lichtenstein, L., Neuberg, D., Catalano, P., Freeman, G.J., Sharpe, A.H., McDermott, D.F., Van Allen, E.M., Signoretti, S., Wu, C.J., Shukla, S.A., Choueiri, T.K.: Interplay of somatic alterations and immune infiltration modulates response to PD-1 blockade in advanced clear cell renal cell carcinoma. Nat Med. 26, 909–918 (2020). https://doi.org/10.1038/s41591-020-0839-y.
53. Hakimi, A.A., Reznik, E., Lee, C.-H., Creighton, C.J., Brannon, A.R., Luna, A., Aksoy, B.A., Liu, E.M., Shen, R., Lee, W., Chen, Y., Stirdivant, S.M., Russo, P., Chen, Y.-B., Tickoo, S.K., Reuter, V.E., Cheng, E.H., Sander, C., Hsieh, J.J.: An Integrated Metabolic Atlas of Clear Cell Renal Cell Carcinoma. Cancer Cell. 29, 104–116 (2016). https://doi.org/10.1016/j.ccell.2015.12.004.
54. Kiran, S., Dar, A., Singh, S.K., Lee, K.Y., Dutta, A.: The Deubiquitinase USP46 Is Essential for Proliferation and Tumor Growth of HPV-Transformed Cancers. Molecular Cell. 72, 823-835.e5

(2018). https://doi.org/10.1016/j.molcel.2018.09.019.
55. Gavi, F., Sighinolfi, M.C., Pallotta, G., Assumma, S., Panio, E., Fettucciari, D., Silvestri, A., Russo, P., Bientinesi, R., Foschi, N., Turri, F., Carbonara, U., Ciccarese, C., Iacovelli, R., Nero, C., Rocco, B.: Multiomics in Renal Cell Carcinoma: Current Landscape and Future Directions for Precision Medicine. Curr Urol Rep. 26, 44 (2025). https://doi.org/10.1007/s11934-025-01276-2.
56. Gao, H., Korn, J.M., Ferretti, S., Monahan, J.E., Wang, Y., Singh, M., Zhang, C., Schnell, C., Yang, G., Zhang, Y., Balbin, O.A., Barbe, S., Cai, H., Casey, F., Chatterjee, S., Chiang, D.Y., Chuai, S., Cogan, S.M., Collins, S.D., Dammassa, E., Ebel, N., Embry, M., Green, J., Kauffmann, A., Kowal, C., Leary, R.J., Lehar, J., Liang, Y., Loo, A., Lorenzana, E., Robert McDonald, E., McLaughlin, M.E., Merkin, J., Meyer, R., Naylor, T.L., Patawaran, M., Reddy, A., Röelli, C., Ruddy, D.A., Salangsang, F., Santacroce, F., Singh, A.P., Tang, Y., Tinetto, W., Tobler, S., Velazquez, R., Venkatesan, K., Von Arx, F., Wang, H.Q., Wang, Z., Wiesmann, M., Wyss, D., Xu, F., Bitter, H., Atadja, P., Lees, E., Hofmann, F., Li, E., Keen, N., Cozens, R., Jensen, M.R., Pryer, N.K., Williams, J.A., Sellers, W.R.: High-throughput screening using patient-derived tumor xenografts to predict clinical trial drug response. Nat Med. 21, 1318–1325 (2015). https://doi.org/10.1038/nm.3954.
57. Tumkur Sitaram, R., Landström, M., Roos, G., Ljungberg, B.: Significance of PI3K signalling pathway in clear cell renal cell carcinoma in relation to VHL and HIF status. J Clin Pathol. 74, 216–222 (2021). https://doi.org/10.1136/jclinpath-2020-206693.
58. Sanchez-Vega, F., Mina, M., Armenia, J., Chatila, W.K., Luna, A., La, K.C., Dimitriadoy, S., Liu, D.L., Kantheti, H.S., Saghafinia, S., Chakravarty, D., Daian, F., Gao, Q., Bailey, M.H., Liang, W.-W., Foltz, S.M., Shmulevich, I., Ding, L., Heins, Z., Ochoa, A., Gross, B., Gao, J., Zhang, H., Kundra, R., Kandoth, C., Bahceci, I., Dervishi, L., Dogrusoz, U., Zhou, W., Shen, H., Laird, P.W., Way, G.P., Greene, C.S., Liang, H., Xiao, Y., Wang, C., Iavarone, A., Berger, A.H., Bivona, T.G., Lazar, A.J., Hammer, G.D., Giordano, T., Kwong, L.N., McArthur, G., Huang, C., Tward, A.D., Frederick, M.J., McCormick, F., Meyerson, M., Caesar-Johnson, S.J., Demchok, J.A., Felau, I., Kasapi, M., Ferguson, M.L., Hutter, C.M., Sofia, H.J., Tarnuzzer, R., Wang, Z., Yang, L., Zenklusen, J.C., Zhang, J. (Julia), Chudamani, S., Liu, J., Lolla, L., Naresh, R., Pihl, T., Sun, Q., Wan, Y., Wu, Y., Cho, J., DeFreitas, T., Frazer, S., Gehlenborg, N., Getz, G., Heiman, D.I., Kim, J., Lawrence, M.S., Lin, P., Meier, S., Noble, M.S., Saksena, G., Voet, D., Zhang, H., Bernard, B., Chambwe, N., Dhankani, V., Knijnenburg, T., Kramer, R., Leinonen, K., Liu, Y., Miller, M., Reynolds, S., Shmulevich, I., Thorsson, V., Zhang, W., Akbani, R., Broom, B.M., Hegde, A.M., Ju, Z., Kanchi, R.S., Korkut, A., Li, J., Liang, H., Ling, S., Liu, W., Lu, Y., Mills, G.B., Ng, K.-S., Rao, A., Ryan, M., Wang, J., Weinstein, J.N., Zhang, J., Abeshouse, A., Armenia, J., Chakravarty, D., Chatila, W.K., De Bruijn, I., Gao, J., Gross, B.E., Heins, Z.J., Kundra, R., La, K., Ladanyi, M., Luna, A., Nissan, M.G., Ochoa, A., Phillips, S.M., Reznik, E., Sanchez-Vega, F., Sander, C., Schultz, N., Sheridan, R., Sumer, S.O., Sun, Y., Taylor, B.S., Wang, J., Zhang, H., Anur, P., Peto, M., Spellman, P., Benz, C., Stuart, J.M., Wong, C.K., Yau, C., Hayes, D.N., Parker, J.S., Wilkerson, M.D., Ally, A., Balasundaram, M., Bowlby, R., Brooks, D., Carlsen, R., Chuah, E., Dhalla, N., Holt, R., Jones, S.J.M., Kasaian, K., Lee, D., Ma, Y., Marra, M.A., Mayo, M., Moore, R.A., Mungall, A.J., Mungall, K., Robertson, A.G., Sadeghi, S., Schein, J.E., Sipahimalani, P., Tam, A., Thiessen, N., Tse, K., Wong, T., Berger, A.C., Beroukhim, R., Cherniack, A.D., Cibulskis, C., Gabriel, S.B., Gao, G.F., Ha, G., Meyerson, M., Schumacher, S.E., Shih, J., Kucherlapati, M.H., Kucherlapati, R.S., Baylin, S., Cope, L., Danilova, L., Bootwalla, M.S., Lai, P.H., Maglinte, D.T., Van Den Berg, D.J., Weisenberger, D.J., Auman, J.T., Balu, S., Bodenheimer, T., Fan, C., Hoadley, K.A., Hoyle, A.P., Jefferys, S.R., Jones, C.D., Meng, S., Mieczkowski, P.A., Mose, L.E., Perou, A.H., Perou, C.M., Roach, J., Shi, Y., Simons, J.V., Skelly, T., Soloway, M.G., Tan, D.,

Veluvolu, U., Fan, H., Hinoue, T., Laird, P.W., Shen, H., Zhou, W., Bellair, M., Chang, K., Covington, K., Creighton, C.J., Dinh, H., Doddapaneni, H., Donehower, L.A., Drummond, J., Gibbs, R.A., Glenn, R., Hale, W., Han, Y., Hu, J., Korchina, V., Lee, S., Lewis, L., Li, W., Liu, X., Morgan, M., Morton, D., Muzny, D., Santibanez, J., Sheth, M., Shinbrot, E., Wang, L., Wang, M., Wheeler, D.A., Xi, L., Zhao, F., Hess, J., Appelbaum, E.L., Bailey, M., Cordes, M.G., Ding, L., Fronick, C.C., Fulton, L.A., Fulton, R.S., Kandoth, C., Mardis, E.R., McLellan, M.D., Miller, C.A., Schmidt, H.K., Wilson, R.K., Crain, D., Curley, E., Gardner, J., Lau, K., Mallery, D., Morris, S., Paulauskis, J., Penny, R., Shelton, C., Shelton, T., Sherman, M., Thompson, E., Yena, P., Bowen, J., Gastier-Foster, J.M., Gerken, M., Leraas, K.M., Lichtenberg, T.M., Ramirez, N.C., Wise, L., Zmuda, E., Corcoran, N., Costello, T., Hovens, C., Carvalho, A.L., De Carvalho, A.C., Fregnani, J.H., Longatto-Filho, A., Reis, R.M., Scapulatempo-Neto, C., Silveira, H.C.S., Vidal, D.O., Burnette, A., Eschbacher, J., Hermes, B., Noss, A., Singh, R., Anderson, M.L., Castro, P.D., Ittmann, M., Huntsman, D., Kohl, B., Le, X., Thorp, R., Andry, C., Duffy, E.R., Lyadov, V., Paklina, O., Setdikova, G., Shabunin, A., Tavobilov, M., McPherson, C., Warnick, R., Berkowitz, R., Cramer, D., Feltmate, C., Horowitz, N., Kibel, A., Muto, M., Raut, C.P., Malykh, A., Barnholtz-Sloan, J.S., Barrett, W., Devine, K., Fulop, J., Ostrom, Q.T., Shimmel, K., Wolinsky, Y., Sloan, A.E., De Rose, A., Giuliante, F., Goodman, M., Karlan, B.Y., Hagedorn, C.H., Eckman, J., Harr, J., Myers, J., Tucker, K., Zach, L.A., Deyarmin, B., Hu, H., Kvecher, L., Larson, C., Mural, R.J., Somiari, S., Vicha, A., Zelinka, T., Bennett, J., Iacocca, M., Rabeno, B., Swanson, P., Latour, M., Lacombe, L., Têtu, B., Bergeron, A., McGraw, M., Staugaitis, S.M., Chabot, J., Hibshoosh, H., Sepulveda, A., Su, T., Wang, T., Potapova, O., Voronina, O., Desjardins, L., Mariani, O., Roman-Roman, S., Sastre, X., Stern, M.-H., Cheng, F., Signoretti, S., Berchuck, A., Bigner, D., Lipp, E., Marks, J., McCall, S., McLendon, R., Secord, A., Sharp, A., Behera, M., Brat, D.J., Chen, A., Delman, K., Force, S., Khuri, F., Magliocca, K., Maithel, S., Olson, J.J., Owonikoko, T., Pickens, A., Ramalingam, S., Shin, D.M., Sica, G., Van Meir, E.G., Zhang, H., Eijckenboom, W., Gillis, A., Korpershoek, E., Looijenga, L., Oosterhuis, W., Stoop, H., Van Kessel, K.E., Zwarthoff, E.C., Calatozzolo, C., Cuppini, L., Cuzzubbo, S., DiMeco, F., Finocchiaro, G., Mattei, L., Perin, A., Pollo, B., Chen, C., Houck, J., Lohavanichbutr, P., Hartmann, A., Stoehr, C., Stoehr, R., Taubert, H., Wach, S., Wullich, B., Kycler, W., Murawa, D., Wiznerowicz, M., Chung, K., Edenfield, W.J., Martin, J., Baudin, E., Bubley, G., Bueno, R., De Rienzo, A., Richards, W.G., Kalkanis, S., Mikkelsen, T., Noushmehr, H., Scarpace, L., Girard, N., Aymerich, M., Campo, E., Giné, E., Guillermo, A.L., Van Bang, N., Hanh, P.T., Phu, B.D., Tang, Y., Colman, H., Evason, K., Dottino, P.R., Martignetti, J.A., Gabra, H., Juhl, H., Akeredolu, T., Stepa, S., Hoon, D., Ahn, K., Kang, K.J., Beuschlein, F., Breggia, A., Birrer, M., Bell, D., Borad, M., Bryce, A.H., Castle, E., Chandan, V., Cheville, J., Copland, J.A., Farnell, M., Flotte, T., Giama, N., Ho, T., Kendrick, M., Kocher, J.-P., Kopp, K., Moser, C., Nagorney, D., O'Brien, D., O'Neill, B.P., Patel, T., Petersen, G., Que, F., Rivera, M., Roberts, L., Smallridge, R., Smyrk, T., Stanton, M., Thompson, R.H., Torbenson, M., Yang, J.D., Zhang, L., Brimo, F., Ajani, J.A., Gonzalez, A.M.A., Behrens, C., Bondaruk, J., Broaddus, R., Czerniak, B., Esmaeli, B., Fujimoto, J., Gershenwald, J., Guo, C., Lazar, A.J., Logothetis, C., Meric-Bernstam, F., Moran, C., Ramondetta, L., Rice, D., Sood, A., Tamboli, P., Thompson, T., Troncoso, P., Tsao, A., Wistuba, I., Carter, C., Haydu, L., Hersey, P., Jakrot, V., Kakavand, H., Kefford, R., Lee, K., Long, G., Mann, G., Quinn, M., Saw, R., Scolyer, R., Shannon, K., Spillane, A., Stretch, J., Synott, M., Thompson, J., Wilmott, J., Al-Ahmadie, H., Chan, T.A., Ghossein, R., Gopalan, A., Levine, D.A., Reuter, V., Singer, S., Singh, B., Tien, N.V., Broudy, T., Mirsaidi, C., Nair, P., Drwiega, P., Miller, J., Smith, J., Zaren, H., Park, J.-W., Hung, N.P., Kebebew, E., Linehan, W.M., Metwalli, A.R., Pacak, K., Pinto, P.A., Schiffman, M., Schmidt, L.S., Vocke, C.D., Wentzensen, N., Worrell, R., Yang, H., Moncrieff, M., Goparaju, C., Melamed, J., Pass, H.,

Botnariuc, N., Caraman, I., Cernat, M., Chemencedji, I., Clipca, A., Doruc, S., Gorincioi, G., Mura, S., Pirtac, M., Stancul, I., Tcaciuc, D., Albert, M., Alexopoulou, I., Arnaout, A., Bartlett, J., Engel, J., Gilbert, S., Parfitt, J., Sekhon, H., Thomas, G., Rassl, D.M., Rintoul, R.C., Bifulco, C., Tamakawa, R., Urba, W., Hayward, N., Timmers, H., Antenucci, A., Facciolo, F., Grazi, G., Marino, M., Merola, R., De Krijger, R., Gimenez-Roqueplo, A.-P., Piché, A., Chevalier, S., McKercher, G., Birsoy, K., Barnett, G., Brewer, C., Farver, C., Naska, T., Pennell, N.A., Raymond, D., Schilero, C., Smolenski, K., Williams, F., Morrison, C., Borgia, J.A., Liptay, M.J., Pool, M., Seder, C.W., Junker, K., Omberg, L., Dinkin, M., Manikhas, G., Alvaro, D., Bragazzi, M.C., Cardinale, V., Carpino, G., Gaudio, E., Chesla, D., Cottingham, S., Dubina, M., Moiseenko, F., Dhanasekaran, R., Becker, K.-F., Janssen, K.-P., Slotta-Huspenina, J., Abdel-Rahman, M.H., Aziz, D., Bell, S., Cebulla, C.M., Davis, A., Duell, R., Elder, J.B., Hilty, J., Kumar, B., Lang, J., Lehman, N.L., Mandt, R., Nguyen, P., Pilarski, R., Rai, K., Schoenfield, L., Senecal, K., Wakely, P., Hansen, P., Lechan, R., Powers, J., Tischler, A., Grizzle, W.E., Sexton, K.C., Kastl, A., Henderson, J., Porten, S., Waldmann, J., Fassnacht, M., Asa, S.L., Schadendorf, D., Couce, M., Graefen, M., Huland, H., Sauter, G., Schlomm, T., Simon, R., Tennstedt, P., Olabode, O., Nelson, M., Bathe, O., Carroll, P.R., Chan, J.M., Disaia, P., Glenn, P., Kelley, R.K., Landen, C.N., Phillips, J., Prados, M., Simko, J., Smith-McCune, K., VandenBerg, S., Roggin, K., Fehrenbach, A., Kendler, A., Sifri, S., Steele, R., Jimeno, A., Carey, F., Forgie, I., Mannelli, M., Carney, M., Hernandez, B., Campos, B., Herold-Mende, C., Jungk, C., Unterberg, A., Von Deimling, A., Bossler, A., Galbraith, J., Jacobus, L., Knudson, M., Knutson, T., Ma, D., Milhem, M., Sigmund, R., Godwin, A.K., Madan, R., Rosenthal, H.G., Adebamowo, C., Adebamowo, S.N., Boussioutas, A., Beer, D., Giordano, T., Mes-Masson, A.-M., Saad, F., Bocklage, T., Landrum, L., Mannel, R., Moore, K., Moxley, K., Postier, R., Walker, J., Zuna, R., Feldman, M., Valdivieso, F., Dhir, R., Luketich, J., Pinero, E.M.M., Quintero-Aguilo, M., Carlotti, C.G., Dos Santos, J.S., Kemp, R., Sankarankuty, A., Tirapelli, D., Catto, J., Agnew, K., Swisher, E., Creaney, J., Robinson, B., Shelley, C.S., Godwin, E.M., Kendall, S., Shipman, C., Bradford, C., Carey, T., Haddad, A., Moyer, J., Peterson, L., Prince, M., Rozek, L., Wolf, G., Bowman, R., Fong, K.M., Yang, I., Korst, R., Rathmell, W.K., Fantacone-Campbell, J.L., Hooke, J.A., Kovatich, A.J., Shriver, C.D., DiPersio, J., Drake, B., Govindan, R., Heath, S., Ley, T., Van Tine, B., Westervelt, P., Rubin, M.A., Lee, J.I., Aredes, N.D., Mariamidze, A., Van Allen, E.M., Cherniack, A.D., Ciriello, G., Sander, C., Schultz, N.: Oncogenic Signaling Pathways in The Cancer Genome Atlas. Cell. 173, 321-337.e10 (2018). https://doi.org/10.1016/j.cell.2018.03.035.

59. Shroff, E.H., Eberlin, L.S., Dang, V.M., Gouw, A.M., Gabay, M., Adam, S.J., Bellovin, D.I., Tran, P.T., Philbrick, W.M., Garcia-Ocana, A., Casey, S.C., Li, Y., Dang, C.V., Zare, R.N., Felsher, D.W.: MYC oncogene overexpression drives renal cell carcinoma in a mouse model through glutamine metabolism. Proc. Natl. Acad. Sci. U.S.A. 112, 6539–6544 (2015). https://doi.org/10.1073/pnas.1507228112.

Supplementary Files

This is a list of supplementary files associated with this preprint. Click to download.

- supplementary.docx